

DETAILEMASTER: CAN YOUR TEXT-TO-IMAGE MODEL HANDLE LONG PROMPTS?

Qirui Jiao^{1*}, Daoyuan Chen^{2*}, Yilun Huang², Xika Lin³, Ying Shen^{1†}, Yaliang Li^{2†}

¹Sun Yat-Sen University, Shenzhen, China

²Alibaba Group, Hangzhou, China

³Worcester Polytechnic Institute

jiaoqr3@mail2.sysu.edu.cn, sheny76@mail.sysu.edu.cn
 {daoyuanchen.cdy, lielin.hyl, yaliang.li}@alibaba-inc.com

ABSTRACT

While recent text-to-image (T2I) models show impressive capabilities in synthesizing images from brief descriptions, their performance significantly degrades when confronted with long, detail-intensive prompts required in professional applications. We present **DETAILEMASTER**, the first comprehensive benchmark specifically designed to evaluate T2I models’ systematic abilities to handle extended textual inputs that contain complex compositional requirements. Our benchmark introduces four critical evaluation dimensions: Character Attributes, Structured Character Locations, Multi-Dimensional Scene Attributes, and Spatial/Interactive Relationships. The benchmark comprises long and detail-rich prompts averaging 284.89 tokens, with high quality validated by expert annotators. Evaluation on 7 general-purpose and 5 long-prompt-optimized T2I models reveals critical performance limitations: state-of-the-art models achieve merely $\sim 50\%$ accuracy in key dimensions like attribute binding and spatial reasoning, while all models showing progressive performance degradation as prompt length increases. Our analysis reveals fundamental limitations in compositional reasoning, demonstrating that current encoders flatten complex grammatical structures and that diffusion models suffer from attribute leakage under detail-intensive conditions. We open-source our dataset, data curation code, and evaluation tools to advance detail-rich T2I generation and enable applications previously hindered by the lack of a dedicated benchmark.

1 INTRODUCTION

While recent advancements in text-to-image (T2I) generation have produced high-fidelity images and practical applications (Betker et al., 2023; Esser et al., 2024; Labs, 2024; Podell et al., 2023), current models remain primarily optimized for short textual inputs. They often struggle with long, complex prompts (see Figure 1 and Appendix P for failure cases), which may consist of hundreds of tokens and contain rich details (e.g., character attributes, spatial relationships, and scene properties).

The limitations of T2I models in faithfully following long prompts can be attributed to four constraints: 1) **Training data bias.** Models are primarily trained on short prompts (e.g., COCO (Lin et al., 2014) averaging 10.5 tokens, CC12M (Changpinyo et al., 2021) averaging 20.2 tokens), which reinforces a preference for concise inputs. 2) **Structural comprehension deficiency.** Most text encoders fail to adequately parse hierarchical descriptions involving multiple objects, attributes, and their spatial relationships, which results in incorrect information segmentation and attribute misalignment. 3) **Detail overload.** When prompts contain excessive descriptive details on a single subject, models tend to omit or distort key details. 4) **Token length constraints.** Most encoders impose strict upper bounds on input tokens (e.g., CLIP’s 77-token limit (Radford et al., 2021)).

*Equal contribution. †Corresponding author.

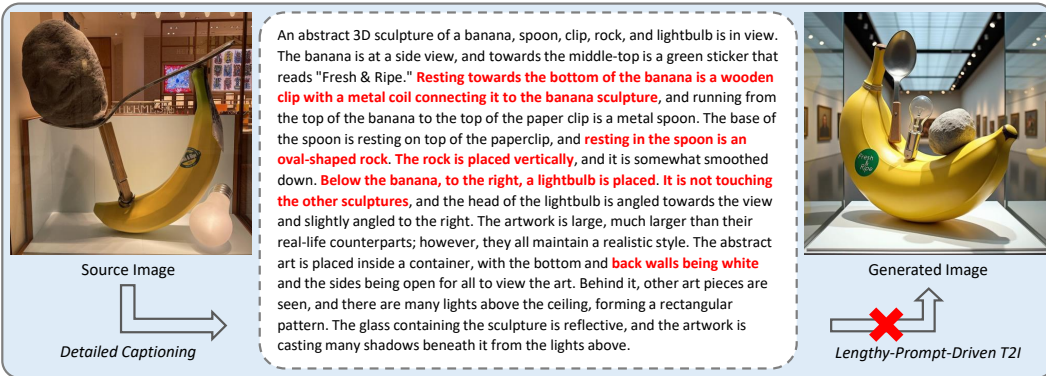


Figure 1: Text-to-image errors in long prompt scenario (with FLUX.1-dev). Real source image (left), detailed caption/prompt (middle), and generated image (right). Red text indicates failure points.

Faithfully interpreting long prompts is a critical capability in many practical scenarios where users have extensive requirements, such as interactive media, visual storytelling, scientific visualization, industrial prototyping, and so on (Cao et al., 2025; Huang et al., 2016; Wu et al., 2024; Xing et al., 2023). Existing evaluations of T2I models have examined their capabilities across multiple dimensions, including image-text alignment, attribute binding, and human preference. However, these evaluations predominantly rely on short prompts. Only a few existing benchmarks involve long-prompt scenarios (Hu et al., 2024; Liu et al., 2025), but they remain limited by constrained token lengths (typically around 100 tokens) and lack detailed attribute descriptions and scene context.

To rigorously evaluate T2I models on long prompts, we introduce **DETAILMASTER**, a novel benchmark along with a robust evaluation protocol. This benchmark assesses prompt adherence across four critical dimensions, specifically designed to target two challenges: structural comprehension deficiency (via **Character Locations** and **Spatial/Interactive Relationships**) and detail overload (via **Character Attributes** and **Scene Attributes**). The prompts in our benchmark are derived from existing detailed captions (Onoe et al., 2024; Pont-Tuset et al., 2020), which we further refine by augmenting missing details, resulting in an average token length of 284.89. To ensure high quality, human experts are engaged to evaluate our benchmark, confirming its high standard. For the evaluation protocol, we develop specialized assessment mechanisms for each category of attributes, enabling systematic evaluation of models' compositional T2I abilities in long-prompt scenarios.

Using our **DETAILMASTER** benchmark, we investigate 7 general-purpose models, including state-of-the-art (SOTA) models FLUX (Labs, 2024) and GPT Image-1 (OpenAI, 2025), along with 5 specialized models optimized for long prompts. While our analysis validates enhanced competencies in recent models over older baselines, it also uncovers critical failure points. We identify a consistent struggle with fine-grained compositional elements, including character attributes, spatial positioning, and entity relationships. A statistical analysis confirms a clear difficulty hierarchy, with **Character Locations** and **Person Attributes** proving the most challenging. Furthermore, we find that performance gains are not merely a function of longer context windows; training on detail-rich, longer prompts is essential. Furthermore, the optimized models' performance is heavily constrained by their backbone architectures. And there is a consistent degradation in prompt adherence as prompt length increases, highlighting fundamental challenges in handling long prompts.

In summary, our contributions are three-fold: 1) We propose the **DETAILMASTER** benchmark, featuring a comprehensive dataset and a robust evaluation protocol to systematically assess the prompt adherence of T2I models in long-prompt scenarios. 2) We conduct extensive comparisons on both popular T2I models and those specifically optimized for long prompts, yielding several insights: current models fail at complex compositional tasks and show a degradation in adherence as prompt length increases; progress in long-prompt adherence is driven less by expanded context windows and more by crucial factors such as long-prompt training and iterative decomposition. 3) We open-source all data and code (<https://github.com/modelscope/data-juicer/tree/DetailMaster>) to facilitate future research in text-to-image generation for long, detail-rich prompts.

Table 1: Comparison of data composition between **DETAILMASTER** and other benchmarks. Detailed statistical analysis provided in Section 5.1.

Benchmark	# Prompts	# Nouns	Character		# Scene Attributes	# Entity Relationships	Avg. Tokens
			# Attributes	# Locations			
HRS-Comp (Bakr et al., 2023)	3004	620	1000	N/A	N/A	2000	16.43
T2I-CompBench (Huang et al., 2023)	6000	2316	4000	N/A	N/A	2000	12.65
DensePrompts (Liu et al., 2025)	7061	4913	N/A	N/A	N/A	N/A	100.04
DPG-Bench (Hu et al., 2024)	1065	4286	5020	N/A	329	2593	83.91
DETAILMASTER (Ours)	4116	5165	37165	6910	12330	18526	284.89

2 RELATED WORKS

Text-to-image models. Text-to-image (T2I) generation aims to synthesize semantically aligned images conditioned on textual descriptions. Initial endeavors use Generative Adversarial Networks (GANs) (Goodfellow et al., 2014), employing a generator-discriminator framework to produce images. Subsequent advancements introduce autoregressive models that treat image generation as a sequence prediction task, including DALL-E (Ramesh et al., 2021) and Parti (Yu et al., 2022). More recently, diffusion-based models (Ho et al., 2020) have emerged as a powerful paradigm. These models, including DALL-E 2 (Ramesh et al., 2022), Imagen (Saharia et al., 2022), and Stable Diffusion (Rombach et al., 2022), operate by iteratively denoising to produce coherent images. Beyond this, flow-based models such as Stable Diffusion 3.5 (Esser et al., 2024) and FLUX (Labs, 2024) use flow matching (Lipman et al., 2022) techniques to learn direct transformations from noise to images, reducing sampling complexity and improving efficiency. Furthermore, the proprietary models Gemini 2.0 Flash (Google, 2025) and GPT Image-1 (OpenAI, 2025) also show SOTA level performance.

Benchmarks for text-to-image generation. Early evaluations for T2I generation primarily use datasets such as CUB Birds (Wah et al., 2011) and Oxford Flowers (Nilsback & Zisserman, 2008), which have limited diversity and simple prompts. Recently, benchmarks such as DrawBench (Saharia et al., 2022), HRS-Bench (Bakr et al., 2023) and T2I-CompBench (Huang et al., 2023) introduce prompts aimed at compositional generation, including object presence, attribute binding, and spatial relationships. To measure the alignment between generated images and every detail within the prompts, benchmarks such as TIFA (Hu et al., 2023) and Gecko (Wiles et al., 2024) decompose prompts into elemental components and generate corresponding questions to assess model fidelity. Moreover, benchmarks such as GenAI-Bench (Li et al., 2024a), RichHF18K (Liang et al., 2024) and HPS v2 (Wu et al., 2023c) aim to train preference-aligned evaluators that reflect human judgment. However, these benchmarks predominantly focus on short prompts, neglecting the challenges of longer, complex inputs that are prone to issues like attribute misalignment.

T2I models for long prompt. To enhance T2I models’ ability to follow long prompts (those exceeding the 77-token limit of the CLIP text encoder), some studies employ large language models (LLMs) as text encoders to improve semantic extraction. Representative models such as Imagen (Saharia et al., 2022), DeepFloyd IF (at StabilityAI, 2023), and advanced approaches like Stable Diffusion 3.5 (Esser et al., 2024) and FLUX (Labs, 2024) adopt frozen T5 (Raffel et al., 2020) as their text encoder, strengthening text-image alignment. Beyond this, ParaDiffusion (Wu et al., 2023a) uses a frozen Llama V2 (Touvron et al., 2023) as its text encoder and constructs a training dataset of long prompts to enhance comprehension. LLM4GEN (Liu et al., 2025) introduces an adapter to fuse features from multiple text encoders (e.g., T5 and CLIP) and proposes a specialized loss to penalize attribute mismatch. ELLA (Hu et al., 2024) incorporates a trainable mapper after the LLM-based text encoder to improve information extraction from long prompts. LongAlign (Liu et al., 2024) decomposes long prompts into individual sentences for separate encoding, while also enabling preference optimization for long-text alignment. LLM Blueprint (Gani et al., 2023) extracts object details from long prompts using an LLM, then employs layout-to-image generation and an iterative refinement scheme for image synthesis. However, due to the scarcity of benchmarks for long-prompt-driven image generation, these methods lack fair comparison.

Benchmarks for long-prompt-driven T2I generation. Current benchmarks for long-prompt-driven image generation remain scarce. DensePrompts (Liu et al., 2025) collects 100 detailed web images, using GPT-4V (Achiam et al., 2023b) to generate attribute-rich descriptions. DPG-Bench (Hu et al., 2024) aggregates multi-short-prompt annotations from existing datasets and employs GPT-4 (Achiam et al., 2023a) to synthesize them into long descriptions. However, these bench-

marks exhibit critical limitations: 1) oversimplified evaluation, relying on CLIP Score (Hessel et al., 2021) or binary feature verification via multimodal large language model (MLLMs), which fail to assess fine-grained and compositional accuracy; 2) constrained prompt length and details, deriving prompts through LLM extraction and failing to match real-world long-prompt complexity. To address these issues, we propose **DETAILMASTER**, a novel benchmark featuring longer prompts along with a fine-grained evaluation protocol to assess T2I generation under complex long-prompt scenarios. As evidenced in Table 1, our benchmark advances prior works through extended prompts, enlarged attribute sets, and more comprehensive evaluation objectives.

3 THE DETAILMASTER BENCHMARK

3.1 DATASET CONSTRUCTION

3.1.1 OVERVIEW

To better simulate the challenges in long-prompt scenarios, we require prompts of sufficient length and rich details. Hence, we leverage existing human-annotated detailed captioning datasets, where each sample comprises an image paired with fine-grained textual descriptions, including DOCCI (Onoe et al., 2024) and Localized Narratives (Flickr30k (Young et al., 2014) and COCO subsets) (Pont-Tuset et al., 2020). While these datasets already provide precise object descriptions with an average token length of 68.4, their coverage is still incomplete. To enhance the image description quality and obtain optimal prompts, we design a robust and fine-grained attribute extraction pipeline that systematically captures four categories of key features: 1) **Character Attributes**, where we categorize main characters (objects, animals, persons, and others) and analyze them via class-specific attribute extraction protocols; 2) **Structured Character Locations**, where we employ a nine grid-based spatial partitioning scheme to assign precise positions; 3) **Multi-Dimensional Scene Attributes**, decomposing scenes into background, lighting conditions, and stylistic elements; and 4) **Spatial/Interactive Relationships**, annotating character pairs with geometric (e.g., “dog behind chair”) and dynamic interactions (e.g., “holding”). These extracted attributes are then integrated into the original captions using LLM-based expansion, yielding richly detailed prompts with an average token length of 284.89. The overview of the data generation process is shown in Figure 2. To enhance reusability, our data construction process is also implemented as data processing operators and configurable data recipes within Data-Juicer (Chen et al., 2025a;b).

3.1.2 ATTRIBUTE EXTRACTION PIPELINE

Main character identification. We first need to know what characters are present in each sample. Specifically, we provide an MLLM with both the image and the caption to detect main characters. We then apply sample filtering to retain only instances containing more than four main characters, ensuring as many high-quality features as possible in the final prompt (see Figure 2 ①).

Character localization. For character localization, we generate two bounding box proposals using an MLLM and the open-set detector YOLOE-11L (Wang et al., 2025). We then validate these proposals through a two-stage process. First, if the boxes have an Intersection over Union (IoU) of at least 0.7, we select the larger one. Otherwise, we employ BLIP (Li et al., 2022b) to score each cropped box against the character’s name; we then retain the higher-scoring box unless both scores fall below 0.4 (see Figure 2 ②). Finally, the validated bounding boxes are converted into structured spatial descriptions using the nine-region partitioning scheme detailed in Appendix B.

Character attribute extraction. For character attributes, we implement a hierarchical pipeline. First, an LLM performs text-based extraction by classifying characters (object, animal, person, other) and using category-specific prompts to derive attributes from captions (e.g., material for objects, clothing for persons). Subsequently, a multimodal refinement stage enhances attribute completeness and simulate detail overload. For characters with valid bounding box information, we crop corresponding sub-images and ask an MLLM to supplement the text-derived attribute lists with visually-grounded features (see Figure 2 ③).

Scene attribute extraction. For scene attributes, we employ an MLLM to jointly analyze the source image and the caption for each sample, identifying its background composition, lighting conditions, and stylistic elements (see Figure 2 ④).

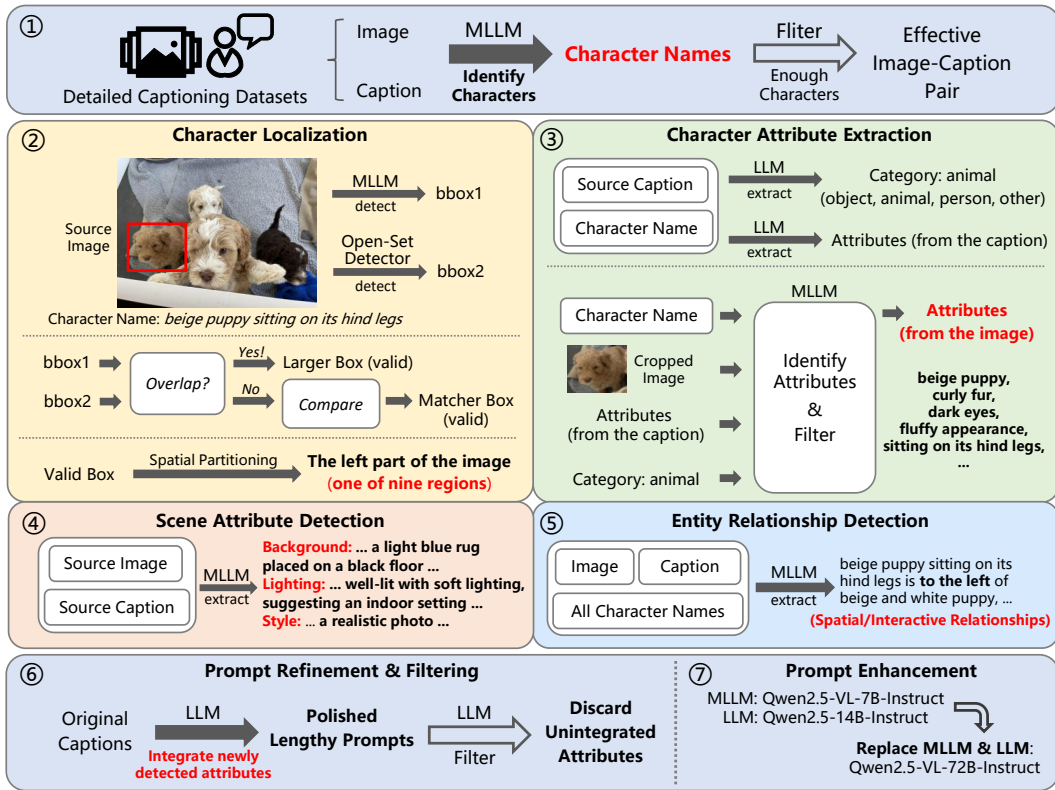


Figure 2: Overview diagram of the data construction process for the **DETAILMASTER** benchmark.

Entity relationship detection. For entity relationships, we input the source image, caption, and all detected characters of each sample into the MLLM. The model then performs relationship parsing to extract all discernible spatial and interactive relationships between entities (see Figure 2 ⑤).

3.1.3 PROMPT REFINEMENT & ENHANCEMENT

Prompt refinement and filtering. Following the attribute extraction, we implement a prompt refinement pipeline to transform the original captions into detail-rich long prompts. For each sample, we enumerate all identified main characters and employ an LLM to incorporate all their attributes and locations into the original caption. Subsequently, the same LLM integrates the sample’s scene attributes and spatial/interactive relationships to produce the refined prompt.

Beyond prompt refinement, the extracted attributes also form the basis of our evaluation metrics. To ensure metric accuracy, we implement an attribute validation mechanism where an LLM verifies the presence of each attribute in the refined prompt, filtering out any unincorporated attributes. In addition, samples with less than 4 valid character-level attributes are filtered out. (see Figure 2 ⑥)

Prompt enhancement. Throughout the attribute extraction and prompt refinement pipeline, we employ Qwen2.5-14B-Instruct (Team, 2024) as our primary LLM and Qwen2.5-VL-7B-Instruct (Team, 2025) as the MLLM. This initial process yields 4,565 detail-rich prompts, with an average token length of 237.53. To achieve higher precision and greater detail, we subsequently reprocess the corresponding 4,565 samples using Qwen2.5-VL-72B-Instruct as both the LLM and the MLLM. This new process generates an improved dataset containing 4,116 prompts with an average token length of 284.89. (see in Figure 2 ⑦)

3.2 EVALUATION PROTOCOL

3.2.1 OVERVIEW

Evaluating compositional T2I generation proves inherently difficult, as it demands fine-grained cross-modal understanding between textual prompts and generated images. Popular approaches typically employ object detection models for spatial verification, vision-language models for image-text alignment (Hessel et al., 2021), and MLLMs for attribute verification (Cho et al., 2023; Huang et al., 2023). However, these methods often yield coarse-grained and noisy assessments, compromising evaluation accuracy. To address these limitations, we develop a robust multi-stage evaluation pipeline that systematically assesses the accuracy of all four categories of attributes.

3.2.2 EVALUATION METRICS

Our evaluation framework is built upon the four categories of attributes that we previously extract. For the “**Character Attributes**” metric, we calculate it as the ratio of correctly rendered attributes to the total number of specified attributes for each character category (i.e., object, animal, and person). The “**Character Locations**” metric assesses accuracy by computing the proportion of characters positioned correctly relative to the total number of annotated characters. For “**Entity Relationships**”, we calculate the percentage of correctly rendered relationships among all those described in the prompt. These three metrics quantify the model’s performance on attribute-level details, specifically targeting mismatches and omissions. For the “**Scene Attributes**” metric, we compute accuracy for background, lighting, and style, evaluating overall image fidelity in long prompt scenarios.

Our main evaluations are conducted on the full version of our **DETAILMASTER**, comprising 4,116 prompts. Additionally, we design a mini version of our benchmark to facilitate rapid evaluation for researchers, which consists of 800 detail-rich prompts. The details are in Appendix L.

3.2.3 EVALUATION PIPELINE

We introduce a multi-step evaluation pipeline to systematically assess the compositional generation capabilities of T2I models. First, we instruct the T2I models with prompts from our **DETAILMASTER** benchmark to generate corresponding image sets. Next, we detect and localize the characters present in the generated images. Subsequently, we conduct a rigorous quantitative evaluation across our four critical dimensions, deriving accuracy rates for each evaluated model. Further details of the evaluation pipeline are provided in Appendix F.

On the Robustness of an MLLM-based Evaluator. While leveraging a single MLLM family (i.e., Qwen) for both data curation and evaluation could raise concerns about potential self-enhancement bias, we argue this risk is mitigated for two key reasons. First, our data construction is heavily grounded by auxiliary tools like open-set object detectors and guided by original human-annotated captions, breaking a purely end-to-end LLM pipeline. Second, as detailed in our robustness analysis (Appendix I), re-evaluating all models with a distinct MLLM (i.e., InternVL) preserves the relative model rankings and core conclusions. This confirms that **DETAILMASTER** measures a general compositional capability rather than an affinity for a specific model’s idiosyncrasies.

4 EXPERIMENTS

4.1 EXPERIMENTAL SETUP

We evaluate the performance of seven general-purpose models and five long-prompt optimized models. Among the general-purpose models, five are open-source implementations including Stable Diffusion 1.5 (Rombach et al., 2022), SD-XL (Podell et al., 2023), DeepFloyd IF (Saharia et al., 2022), Stable Diffusion 3.5 Large (Esser et al., 2024), and FLUX.1-dev (Labs, 2024), while two are proprietary commercial systems, specifically the image generation modules of Gemini 2.0 Flash (Google, 2025) and GPT-4o (OpenAI, 2025). The long-prompt optimized models include LLM4GEN (Liu et al., 2025), ELLA (Hu et al., 2024), LongAlign (Liu et al., 2024), LLM Blueprint (Gani et al., 2023), and ParaDiffusion (Wu et al., 2023a). Detailed configurations for all the evaluated models are provided in Appendix C. Regarding the evaluation metrics, we assess each model across four

Table 2: Results on the **DETAILMASTER** Benchmark. Values represent accuracy percentages.

(A) General-Purpose Text-to-Image Model									
Model	Backbone	Character Attributes			Character Locations	Scene Attributes			Entity Relationships
		Object	Animal	Person		Background	Light	Style	
SD1.5 (Rombach et al., 2022)	-	20.79	27.69	13.89	8.68	22.02	64.52	80.90	5.88
SD-XL (Podell et al., 2023)	-	24.41	29.54	16.73	10.95	27.52	68.42	68.87	9.83
DeepFloyd IF (at StabilityAI, 2023)	-	31.01	37.47	25.61	14.28	26.26	67.87	86.49	11.95
SD3.5 Large (Esser et al., 2024)	-	48.56	46.20	32.95	33.62	89.61	90.33	95.69	40.03
FLUX.1-dev (Labs, 2024)	-	51.47	45.83	34.91	41.57	95.77	97.05	94.81	47.49
Gemini 2.0 Flash (Google, 2025)	-	55.44	47.84	34.23	44.74	96.69	95.90	97.20	50.78
GPT Image-1 (OpenAI, 2025)	-	59.41	48.04	40.40	53.92	97.50	98.85	97.69	63.07

(B) Long-Prompt Optimized Text-to-Image Model									
Model	Backbone	Character Attributes			Character Locations	Scene Attributes			Entity Relationships
		Object	Animal	Person		Background	Light	Style	
LLM4GEN (Liu et al., 2025)	SD1.5	21.75	29.14	17.20	9.22	25.60	65.71	50.11	7.44
LLM Blueprint (Gani et al., 2023)	SD1.5	21.41	27.01	13.91	18.44	50.89	77.57	64.24	11.60
ELLA (Hu et al., 2024)	SD1.5	34.50	35.14	22.01	15.92	47.12	74.28	40.14	16.64
LongAlign (Liu et al., 2024)	SD1.5	32.95	34.60	15.35	14.89	77.03	87.70	72.27	19.17
ParaDiffusion (Wu et al., 2023a)	SD-XL	35.25	33.28	22.29	20.32	83.65	92.21	67.45	25.50

key generation tasks: Character Attributes, Character Locations, Scene Attributes, and Entity Relationships, enabling systematic assessment of compositional text-to-image generation in long-prompt scenarios. The results are presented in Table 2.

4.2 PERFORMANCE EVALUATIONS ON **DETAILMASTER**

4.2.1 COMPARISONS ACROSS GENERAL-PURPOSE TEXT-TO-IMAGE MODELS

Impact of token length constraints. As shown in Table 2, models employing CLIP as the text encoder (SD1.5 and SD-XL) show significant limitations when handling long prompts due to token length constraints, consistently underperforming across all four tasks. In contrast, DeepFloyd IF, which employs T5 as its text encoder, benefits from an extended input capacity and visibly outperforms the former two models. Nevertheless, its performance remains bad, constrained by both the quality of its short training data and inherent architectural limitations.

Performance ceiling of SOTA models. SD3.5 and FLUX, which combine T5 with enhanced training data and superior model architecture, show improvements over previous models. These two models achieve remarkable performance on “Scene Attributes”, attaining accuracy exceeding 90%, indicating robust scene control capability. However, their performance remains constrained on the other three tasks, suggesting that the absence of explicit training on long prompts limits their adaptability. The proprietary models, Gemini 2.0 Flash and GPT Image-1, outperform all aforementioned open-source models. Nevertheless, their accuracy for “Character Attributes”, “Character Locations”, and “Entity Relationships” also plateaus at around 50%, indicating that even SOTA models have considerable room for improvement in long prompt scenarios.

4.2.2 COMPARISONS ACROSS LONG-PROMPT OPTIMIZED TEXT-TO-IMAGE MODELS

Long prompt training matters more than increasing token capacity. While LLM4GEN uses an adapter to infuse T5 features, its 128-token limit during training fails to address long prompt challenges, leading to slight improvements. ELLA maintains the same token constraint but train with long and complex prompt, yielding more improvements than LLM4GEN. With a similar architecture and training strategy, ParaDiffusion extends the limit to 512 during training, enabling superior performance. Compared to DeepFloyd IF (with same token capacity but conventional training), ParaDiffusion shows better performance across almost all metrics. These results validate that while expanded token capacity provides necessary infrastructure, long prompt training yields greater gains.

Decomposition and iteration mitigates long-prompt challenges. LongAlign decomposes long prompts for separate encoding and trains with long prompts, indirectly increasing the token capacity and achieving notable gains. LLM Blueprint identifies key roles and locations from long prompts, followed by iterative image refinement, yielding notable improvements in “Character Locations”.

Table 3: Attribute accuracy of detected generated characters across models.

Character Attributes	SD-XL	DeepFloyd IF	SD3.5 Large	FLUX.1-dev	Gemini 2.0 Flash	GPT Image-1
Object	79.17	81.19	86.55	89.01	90.06	91.77
Animal	84.27	82.73	89.39	90.37	90.37	92.31
Person	80.65	83.35	89.10	91.06	92.46	94.10
Character Attributes	SD1.5	LLM4GEN	LLM Blueprint	ELLA	LongAlign	ParaDiffusion
Object	74.66	75.62	72.01	82.06	82.58	83.22
Animal	80.30	81.46	79.91	84.55	84.87	84.29
Person	75.93	77.90	71.98	84.55	82.48	83.40

Performance bottlenecks in backbone architectures. Nevertheless, current long-prompt optimized methods predominantly build upon SD1.5 and SD-XL. While these methods show measurable improvements over their baseline counterparts, their overall performance remains unsatisfactory.

4.2.3 ANALYSIS ON KEY GENERATION TASKS

Metric difficulty hierarchy. Notably, “Character Attributes”, “Character Locations”, and “Entity Relationships” remain challenging, while “Scene Attributes” proves easier. We quantitatively establish this hierarchy in Appendix M.

Error source analysis. Our analysis of failure cases (detailed in Appendix M) illuminates the model’s primary weaknesses. The predominant error patterns are: 1) conflicts between spatial instructions and the model’s real-world positional priors; 2) difficulty rendering complex descriptions, including detailed character interactions and intricate apparel; and 3) cascading failures, where initial errors in character attributes preclude the correct generation of entity relationships; 4) errors in scene attributes, typically confined to excessive structural complexity or highly specialized styles.

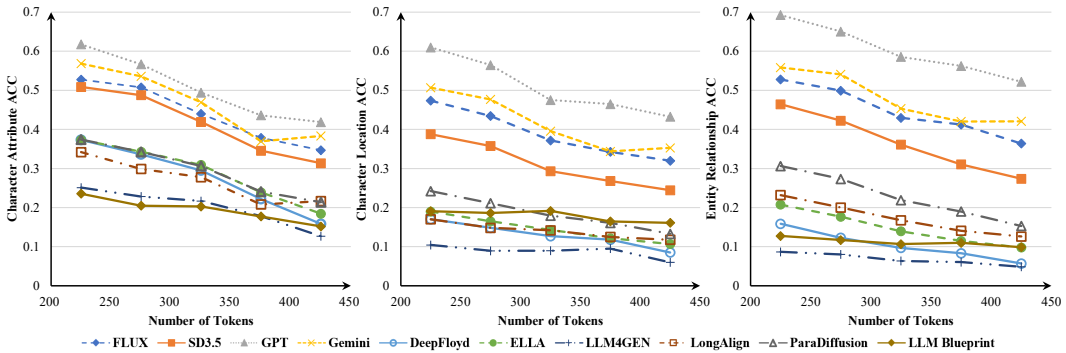


Figure 3: Negative correlation between generation accuracy and prompt token length.

Style degradation from optimization. Interestingly, for the style attribute, the optimized models underperform. This may stem from our benchmark’s bias towards the realistic styles: while SD1.5 naturally aligns with real-world styles, optimizations may introduce undesirable deviations.

Stronger models mitigate attribute misalignment. We assess attribute accuracy exclusively for successfully generated characters to isolate model performance on attribute misalignment from character omission. Table 3 shows that advanced models achieve superior accuracy, demonstrating enhanced prompt comprehension and more precise attribute-character alignment.

4.3 NEGATIVE CORRELATION BETWEEN PROMPT LENGTH AND ADHERENCE.

To better understand the impact of prompt length on text-to-image generation, we analyze the relationship between prompt token length (tokenized using CLIP’s tokenizer) and the accuracy of “Character Attributes”, “Character Locations”, and “Entity Relationships”. We employ five distinct length intervals: below 250, above 400, and three 50-token intervals spanning 250-400. The results, illustrated in Figure 3, show a consistent negative correlation between prompt length and generation accuracy across 10 evaluated models (excluding SD1.5 and SD-XL due to their limited context

windows). This indicates that current T2I models indeed struggle to faithfully follow long prompts, suggesting substantial room for improvement in handling complex prompt scenarios.

Furthermore, our analysis in Appendix N reveals this is not merely an issue of character omission; even for the present characters, the fidelity of attribute alignment also deteriorates with increasing prompt length, highlighting a core failure in attribute binding under detail-intensive conditions.

5 EVALUATION OF DATA QUALITY AND DIVERSITY

5.1 DATA STATISTICS

Our **DETAILMASTER** Benchmark contains 4,116 prompts, covering 5,165 distinct nouns with an average prompt length of 284.89 tokens. The token length distribution reveals: 285 prompts at 100-200, 2,399 prompts at 200-300, 1,151 prompts at 300-400, and 281 prompts exceed 400. Its comprehensive annotations include: 1) “Character Attributes”: 8,597 valid characters annotated with 37,165 distinct features (22,728 for “object”, 4,810 for “animal”, and 9,627 for “person”); 2) “Character Locations”: 6,910 character position annotations; 3) “Scene Attributes”: 4,104 background descriptions, 4,114 lighting descriptions, and 4,112 style descriptions. 4) “Entity Relationships”: 18,526 spatial/interactive relationship annotations. As illustrated in Table 1, our benchmark surpasses existing benchmarks through more comprehensive metrics and longer prompts, offering a more rigorous test for T2I models on long-form instructions.

5.2 HUMAN EVALUATION

To assess the data quality of our **DETAILMASTER** Benchmark, we randomly select 50 samples from each evaluation task (400 in total) and employ two expert annotators to evaluate them, with scores being averaged. The evaluation is based on three criteria: 1) **Task Relevance**: alignment of the prompts and annotations with their designated tasks; 2) **Source Image Fidelity**: alignment of the prompts and annotations with the source images (for hallucination assessment); 3) **Prompt Consistency**: whether the annotations are reflected in the final polished prompts. The results show that 100% of samples meet task relevance requirements, 93.6% maintain visual fidelity with source images, and 97.5% show complete consistency with final polished prompts. These findings validate that our **DETAILMASTER** Benchmark faithfully derives from authentic image-caption pairs, ensuring its validity. Furthermore, the strong alignment mitigates evaluation errors caused by missing attribute descriptions. These results collectively confirm the high quality and robustness of our benchmark. Detailed human evaluation results for specific sub-tasks are provided in Appendix G.

6 FURTHER ANALYSIS AND INSIGHTS

Benchmark Validity and Robustness. We confirm the high fidelity of **DETAILMASTER** through expert human evaluation, which shows near-perfect alignment between our prompts, annotations, and the source images (Appendix G). The robustness of our LLM-based evaluation is established by consistent model rankings and conclusions across a different evaluator and random seeds (Appendix I, J), ensuring that our findings are reproducible and not an artifact of the evaluator choice.

A Hierarchy of Compositional Failure. Our fine-grained metrics reveal a clear difficulty hierarchy for T2I models. Precise spatial reasoning (*Character Locations*) is the most challenging task, which due to conflicts with strong real-world priors, followed by rendering complex *Person Attributes* (Appendix M). In contrast, general *Scene Attributes* like lighting and style are rendered with much higher fidelity. This hierarchy pinpoints critical areas for future research.

Attribute Binding Fails Under High Detail Loads. The negative correlation between prompt length and accuracy (Figure 3) is not merely due to character omission. Our analysis shows that even for the present characters, attribute accuracy degrades as prompts grow longer (Appendix N).

Fostering Broader Adoption. To promote community adoption, we provide a resource-efficient *Mini-Benchmark* for rapid evaluation, which preserves the model ranking trends of the full dataset (Appendix L). Furthermore, we demonstrate the framework’s compatibility with external metrics for assessing orthogonal dimensions such as image aesthetics and safety (Appendix K).

7 DISCUSSION AND CONCLUSION

We introduce **DETAILMASTER**, the first large-scale benchmark for evaluating T2I models on long, detail-intensive prompts. Our evaluations with 12 models reveal a critical performance gap: even SOTA systems exhibit deficiencies in complex compositional generation, with prompt adherence deteriorating as prompt length grows; the primary drivers of enhanced long-prompt adherence are not larger context windows but methods such as long-prompt training and iterative decomposition. We hope **DETAILMASTER** enables more work towards building more precise, controllable, and detail-oriented T2I models, unlocking applications hindered by a lack of compositional fidelity.

Based on our analysis, we hypothesize the failures in long-prompt scenarios are caused by text encoders that “flatten” compositional grammar and diffusion models that permit “attribute leakage.” Direct causal validation of these mechanisms remains an open question, illuminating several avenues for future research: 1) **Structure-Aware Text Encoders**: Developing encoders that explicitly model a prompt’s syntactic or semantic graph structure, rather than treating it as a flat token sequence, to better preserve compositional meaning. 2) **Object-Centric Diffusion Models**: Investigating architectures that learn disentangled, object-centric latent representations (perhaps via specialized attention or binding slots) to mitigate attribute leakage and enforce stricter object-attribute associations. 3) **Curriculum-Based and Data-Centric Training**: Scaling our data generation pipeline to create massive, high-quality datasets for long-prompt training, and exploring curriculum learning that progresses from simple to complex prompts to improve compositional generalization.

REFERENCES

Josh Achiam, Steven Adler, Sandhini Agarwal, Lama Ahmad, Ilge Akkaya, Florencia Leoni Aleman, Diogo Almeida, Janko Altenschmidt, Sam Altman, Shyamal Anadkat, et al. Gpt-4 technical report. *arXiv preprint arXiv:2303.08774*, 2023a.

Josh Achiam, Steven Adler, Sandhini Agarwal, Lama Ahmad, Ilge Akkaya, Florencia Leoni Aleman, Diogo Almeida, Janko Altenschmidt, Sam Altman, Shyamal Anadkat, et al. Gpt-4 technical report. *arXiv preprint arXiv:2303.08774*, 2023b.

DeepFloyd Lab at StabilityAI. DeepFloyd IF: a novel state-of-the-art open-source text-to-image model with a high degree of photorealism and language understanding. <https://www.deepfloyd.ai/deepfloyd-if>, 2023. Retrieved on 2023-11-08.

Eslam Mohamed Bakr, Pengzhan Sun, Xiaoqian Shen, Faizan Farooq Khan, Li Erran Li, and Mohamed Elhoseiny. Hrs-bench: Holistic, reliable and scalable benchmark for text-to-image models. In *Proceedings of the IEEE/CVF International Conference on Computer Vision*, pp. 20041–20053, 2023.

James Betker, Gabriel Goh, Li Jing, Tim Brooks, Jianfeng Wang, Linjie Li, Long Ouyang, Juntang Zhuang, Joyce Lee, Yufei Guo, et al. Improving image generation with better captions. *Computer Science*. <https://cdn.openai.com/papers/dall-e-3.pdf>, 2(3):8, 2023.

Yihan Cao, Siyu Li, Yixin Liu, Zhiling Yan, Yutong Dai, Philip Yu, and Lichao Sun. A survey of ai-generated content (aigc). *ACM Computing Surveys*, 57(5):1–38, 2025.

Soravit Changpinyo, Piyush Sharma, Nan Ding, and Radu Soricut. Conceptual 12m: Pushing web-scale image-text pre-training to recognize long-tail visual concepts. In *Proceedings of the IEEE/CVF conference on computer vision and pattern recognition*, pp. 3558–3568, 2021.

Daoyuan Chen, Yilun Huang, Xuchen Pan, Nana Jiang, Haibin Wang, Yilei Zhang, Ce Ge, Yushuo Chen, Wenhao Zhang, Zhijian Ma, Jun Huang, Wei Lin, Yaliang Li, Bolin Ding, and Jingren Zhou. Data-juicer 2.0: Cloud-scale adaptive data processing for and with foundation models. In *NeurIPS*, 2025a.

Daoyuan Chen, Haibin Wang, Yilun Huang, Ce Ge, Yaliang Li, Bolin Ding, and Jingren Zhou. Data-juicer sandbox: A feedback-driven suite for multimodal data-model co-development. In *ICML*, 2025b.

Zhe Chen, Weiyun Wang, Yue Cao, Yangzhou Liu, Zhangwei Gao, Erfei Cui, Jinguo Zhu, Shenglong Ye, Hao Tian, Zhaoyang Liu, et al. Expanding performance boundaries of open-source multimodal models with model, data, and test-time scaling. *arXiv preprint arXiv:2412.05271*, 2024.

Jaemin Cho, Yushi Hu, Roopal Garg, Peter Anderson, Ranjay Krishna, Jason Baldridge, Mohit Bansal, Jordi Pont-Tuset, and Su Wang. Davidsonian scene graph: Improving reliability in fine-grained evaluation for text-to-image generation. *arXiv preprint arXiv:2310.18235*, 2023.

Gheorghe Comanici, Eric Bieber, Mike Schaeckermann, Ice Pasupat, Noveen Sachdeva, Inderjit Dhillon, Marcel Blstein, Ori Ram, Dan Zhang, Evan Rosen, et al. Gemini 2.5: Pushing the frontier with advanced reasoning, multimodality, long context, and next generation agentic capabilities. *arXiv preprint arXiv:2507.06261*, 2025.

Zhongjie Duan, Lizhou You, Chengyu Wang, Cen Chen, Ziheng Wu, Weining Qian, and Jun Huang. Diffsynth: Latent in-iteration deflickering for realistic video synthesis. In *Joint European Conference on Machine Learning and Knowledge Discovery in Databases*, pp. 332–347. Springer, 2024.

Patrick Esser, Sumith Kulal, Andreas Blattmann, Rahim Entezari, Jonas Müller, Harry Saini, Yam Levi, Dominik Lorenz, Axel Sauer, Frederic Boesel, et al. Scaling rectified flow transformers for high-resolution image synthesis. In *Forty-first international conference on machine learning*, 2024.

Falcons.ai. nsfw-image-detection. https://huggingface.co/Falconsai/nsfw_image_detection, 2023.

Hanan Gani, Shariq Farooq Bhat, Muzammal Naseer, Salman Khan, and Peter Wonka. Llm blueprint: Enabling text-to-image generation with complex and detailed prompts. *arXiv preprint arXiv:2310.10640*, 2023.

Ian J Goodfellow, Jean Pouget-Abadie, Mehdi Mirza, Bing Xu, David Warde-Farley, Sherjil Ozair, Aaron Courville, and Yoshua Bengio. Generative adversarial nets. *Advances in neural information processing systems*, 27, 2014.

Google. Gemini 2.0 flash image generation. <https://ai.google.dev/gemini-api/docs/image-generation#gemini>, 2025.

Jack Hessel, Ari Holtzman, Maxwell Forbes, Ronan Le Bras, and Yejin Choi. Clipscore: A reference-free evaluation metric for image captioning. *arXiv preprint arXiv:2104.08718*, 2021.

Jonathan Ho, Ajay Jain, and Pieter Abbeel. Denoising diffusion probabilistic models. *Advances in neural information processing systems*, 33:6840–6851, 2020.

Xiwei Hu, Rui Wang, Yixiao Fang, Bin Fu, Pei Cheng, and Gang Yu. Ella: Equip diffusion models with llm for enhanced semantic alignment. *arXiv preprint arXiv:2403.05135*, 2024.

Yushi Hu, Benlin Liu, Jungo Kasai, Yizhong Wang, Mari Ostendorf, Ranjay Krishna, and Noah A Smith. Tifa: Accurate and interpretable text-to-image faithfulness evaluation with question answering. In *Proceedings of the IEEE/CVF International Conference on Computer Vision*, pp. 20406–20417, 2023.

Kaiyi Huang, Kaiyue Sun, Enze Xie, Zhenguo Li, and Xihui Liu. T2i-compbench: A comprehensive benchmark for open-world compositional text-to-image generation. *Advances in Neural Information Processing Systems*, 36:78723–78747, 2023.

Ting-Hao Huang, Francis Ferraro, Nasrin Mostafazadeh, Ishan Misra, Aishwarya Agrawal, Jacob Devlin, Ross Girshick, Xiaodong He, Pushmeet Kohli, Dhruv Batra, et al. Visual storytelling. In *Proceedings of the 2016 conference of the North American chapter of the association for computational linguistics: Human language technologies*, pp. 1233–1239, 2016.

Qirui Jiao, Dao yuan Chen, Yilun Huang, Yaliang Li, and Ying Shen. From training-free to adaptive: Empirical insights into mllms’ understanding of detection information. *arXiv preprint arXiv:2401.17981*, 2024.

Qirui Jiao, Daoyuan Chen, Yilun Huang, Bolin Ding, Yaliang Li, and Ying Shen. Img-diff: Contrastive data synthesis for multimodal large language models. In *Proceedings of the Computer Vision and Pattern Recognition Conference*, pp. 9296–9307, 2025.

Jiayi Kuang, Yinghui Li, Chen Wang, Haohao Luo, Ying Shen, and Wenhao Jiang. Express what you see: Can multimodal llms decode visual ciphers with intuitive semiosis comprehension? In *Findings of the Association for Computational Linguistics: ACL 2025*, pp. 12743–12774, 2025a.

Jiayi Kuang, Ying Shen, Jingyou Xie, Haohao Luo, Zhe Xu, Ronghao Li, Yinghui Li, Xianfeng Cheng, Xika Lin, and Yu Han. Natural language understanding and inference with mllm in visual question answering: A survey. *ACM Computing Surveys*, 57(8):1–36, 2025b.

Black Forest Labs. Flux. <https://github.com/black-forest-labs/flux>, 2024.

Baiqi Li, Zhiqiu Lin, Deepak Pathak, Jiayao Emily Li, Xide Xia, Graham Neubig, Pengchuan Zhang, and Deva Ramanan. Genai-bench: A holistic benchmark for compositional text-to-visual generation. In *Synthetic Data for Computer Vision Workshop@ CVPR 2024*, 2024a.

Bo Li, Yuanhan Zhang, Dong Guo, Renrui Zhang, Feng Li, Hao Zhang, Kaichen Zhang, Peiyuan Zhang, Yanwei Li, Ziwei Liu, et al. Llava-onevision: Easy visual task transfer. *arXiv preprint arXiv:2408.03326*, 2024b.

Chenliang Li, Haiyang Xu, Junfeng Tian, Wei Wang, Ming Yan, Bin Bi, Jiabo Ye, Hehong Chen, Guohai Xu, Zheng Cao, et al. mplug: Effective and efficient vision-language learning by cross-modal skip-connections. *arXiv preprint arXiv:2205.12005*, 2022a.

Junnan Li, Dongxu Li, Caiming Xiong, and Steven Hoi. Blip: Bootstrapping language-image pre-training for unified vision-language understanding and generation. In *International conference on machine learning*, pp. 12888–12900. PMLR, 2022b.

Youwei Liang, Junfeng He, Gang Li, Peizhao Li, Arseniy Klimovskiy, Nicholas Carolan, Jiao Sun, Jordi Pont-Tuset, Sarah Young, Feng Yang, et al. Rich human feedback for text-to-image generation. In *Proceedings of the IEEE/CVF Conference on Computer Vision and Pattern Recognition*, pp. 19401–19411, 2024.

Tsung-Yi Lin, Michael Maire, Serge Belongie, James Hays, Pietro Perona, Deva Ramanan, Piotr Dollár, and C Lawrence Zitnick. Microsoft coco: Common objects in context. In *Computer vision–ECCV 2014: 13th European conference, zurich, Switzerland, September 6–12, 2014, proceedings, part v 13*, pp. 740–755. Springer, 2014.

Yaron Lipman, Ricky TQ Chen, Heli Ben-Hamu, Maximilian Nickel, and Matt Le. Flow matching for generative modeling. *arXiv preprint arXiv:2210.02747*, 2022.

Luping Liu, Chao Du, Tianyu Pang, Zehan Wang, Chongxuan Li, and Dong Xu. Improving long-text alignment for text-to-image diffusion models. *arXiv preprint arXiv:2410.11817*, 2024.

Mushui Liu, Yuhang Ma, Zhen Yang, Jun Dan, Yunlong Yu, Zeng Zhao, Zhipeng Hu, Bai Liu, and Changjie Fan. Llm4gen: Leveraging semantic representation of llms for text-to-image generation. In *Proceedings of the AAAI Conference on Artificial Intelligence*, volume 39, pp. 5523–5531, 2025.

Haohao Luo, Jiayi Kuang, Wei Liu, Ying Shen, Jian Luan, and Yang Deng. Browsing like human: A multimodal web agent with experiential fast-and-slow thinking. In *Proceedings of the 63rd Annual Meeting of the Association for Computational Linguistics (Volume 1: Long Papers)*, pp. 14232–14251, 2025.

Maria-Elena Nilsback and Andrew Zisserman. Automated flower classification over a large number of classes. In *2008 Sixth Indian conference on computer vision, graphics & image processing*, pp. 722–729. IEEE, 2008.

Yasumasa Onoe, Sunayana Rane, Zachary Berger, Yonatan Bitton, Jaemin Cho, Roopal Garg, Alexander Ku, Zarana Parekh, Jordi Pont-Tuset, Garrett Tanzer, et al. Doccii: Descriptions of connected and contrasting images. In *European Conference on Computer Vision*, pp. 291–309. Springer, 2024.

OpenAI. Gpt image-1. <https://openai.com/index/introducing-40-image-generation/>, 2025.

Dustin Podell, Zion English, Kyle Lacey, Andreas Blattmann, Tim Dockhorn, Jonas Müller, Joe Penna, and Robin Rombach. Sdxl: Improving latent diffusion models for high-resolution image synthesis. *arXiv preprint arXiv:2307.01952*, 2023.

Jordi Pont-Tuset, Jasper Uijlings, Soravit Changpinyo, Radu Soricut, and Vittorio Ferrari. Connecting vision and language with localized narratives. In *Computer Vision–ECCV 2020: 16th European Conference, Glasgow, UK, August 23–28, 2020, Proceedings, Part V 16*, pp. 647–664. Springer, 2020.

Zhen Qin, Daoyuan Chen, Wenhao Zhang, Liuyi Yao, Yilun Huang, Bolin Ding, Yaliang Li, and Shuguang Deng. The synergy between data and multi-modal large language models: A survey from co-development perspective. *IEEE Transactions on Pattern Analysis and Machine Intelligence*, 47(10):8415–8434, 2025. doi: 10.1109/TPAMI.2025.3576835.

Alec Radford, Jong Wook Kim, Chris Hallacy, Aditya Ramesh, Gabriel Goh, Sandhini Agarwal, Girish Sastry, Amanda Askell, Pamela Mishkin, Jack Clark, et al. Learning transferable visual models from natural language supervision. In *International conference on machine learning*, pp. 8748–8763. PmlR, 2021.

Colin Raffel, Noam Shazeer, Adam Roberts, Katherine Lee, Sharan Narang, Michael Matena, Yanqi Zhou, Wei Li, and Peter J Liu. Exploring the limits of transfer learning with a unified text-to-text transformer. *Journal of machine learning research*, 21(140):1–67, 2020.

Aditya Ramesh, Mikhail Pavlov, Gabriel Goh, Scott Gray, Chelsea Voss, Alec Radford, Mark Chen, and Ilya Sutskever. Zero-shot text-to-image generation. In *International conference on machine learning*, pp. 8821–8831. Pmlr, 2021.

Aditya Ramesh, Prafulla Dhariwal, Alex Nichol, Casey Chu, and Mark Chen. Hierarchical text-conditional image generation with clip latents. *arXiv preprint arXiv:2204.06125*, 1(2):3, 2022.

Robin Rombach, Andreas Blattmann, Dominik Lorenz, Patrick Esser, and Björn Ommer. High-resolution image synthesis with latent diffusion models. In *Proceedings of the IEEE/CVF conference on computer vision and pattern recognition*, pp. 10684–10695, 2022.

Chitwan Saharia, William Chan, Saurabh Saxena, Lala Li, Jay Whang, Emily L Denton, Kamyar Ghasemipour, Raphael Gontijo Lopes, Burcu Karagol Ayan, Tim Salimans, et al. Photorealistic text-to-image diffusion models with deep language understanding. *Advances in neural information processing systems*, 35:36479–36494, 2022.

Qwen Team. Qwen2.5: A party of foundation models, September 2024. URL <https://qwenlm.github.io/blog/qwen2.5/>.

Qwen Team. Qwen2.5-v1, January 2025. URL <https://qwenlm.github.io/blog/qwen2.5-v1/>.

Hugo Touvron, Louis Martin, Kevin Stone, Peter Albert, Amjad Almahairi, Yasmine Babaei, Nikołay Bashlykov, Soumya Batra, Prajjwal Bhargava, Shruti Bhosale, et al. Llama 2: Open foundation and fine-tuned chat models. *arXiv preprint arXiv:2307.09288*, 2023.

Catherine Wah, Steve Branson, Peter Welinder, Pietro Perona, and Serge Belongie. The caltech-ucsd birds-200-2011 dataset. 2011.

Ao Wang, Lihao Liu, Hui Chen, Zijia Lin, Jungong Han, and Guiguang Ding. Yoloe: Real-time seeing anything. *arXiv preprint arXiv:2503.07465*, 2025.

Olivia Wiles, Chuhan Zhang, Isabela Albuquerque, Ivana Kajić, Su Wang, Emanuele Bugliarello, Yasumasa Onoe, Pinelopi Papalampidi, Ira Ktena, Chris Knutson, et al. Revisiting text-to-image evaluation with gecko: On metrics, prompts, and human ratings. *arXiv preprint arXiv:2404.16820*, 2024.

Jianfeng Wu, Yuting Cai, Tingyu Sun, Keer Ma, and Chunfu Lu. Integrating aigc with design: dependence, application, and evolution-a systematic literature review. *Journal of Engineering Design*, pp. 1–39, 2024.

Weijia Wu, Zhuang Li, Yefei He, Mike Zheng Shou, Chunhua Shen, Lele Cheng, Yan Li, Tingting Gao, Di Zhang, and Zhongyuan Wang. Paragraph-to-image generation with information-enriched diffusion model. *arXiv preprint arXiv:2311.14284*, 2023a.

Xiaoshi Wu, Yiming Hao, Keqiang Sun, Yixiong Chen, Feng Zhu, Rui Zhao, and Hongsheng Li. Human preference score v2: A solid benchmark for evaluating human preferences of text-to-image synthesis. *arXiv preprint arXiv:2306.09341*, 2023b.

Xiaoshi Wu, Yiming Hao, Keqiang Sun, Yixiong Chen, Feng Zhu, Rui Zhao, and Hongsheng Li. Human preference score v2: A solid benchmark for evaluating human preferences of text-to-image synthesis. *arXiv preprint arXiv:2306.09341*, 2023c.

Qingqing Xing, Chenghong Zheng, Nan Zhu, and David Yip. Ai-generated content for academic visualization and communication in maker education. In *2023 3rd International Conference on Educational Technology (ICET)*, pp. 52–56. IEEE, 2023.

Jiazheng Xu, Xiao Liu, Yuchen Wu, Yuxuan Tong, Qinkai Li, Ming Ding, Jie Tang, and Yuxiao Dong. Imagereward: Learning and evaluating human preferences for text-to-image generation. *Advances in Neural Information Processing Systems*, 36:15903–15935, 2023.

Zhe Xu, Daoyuan Chen, Zhenqing Ling, Yaliang Li, and Ying Shen. Mindgym: What matters in question synthesis for thinking-centric fine-tuning? In *NeurIPS*, 2025.

Peter Young, Alice Lai, Micah Hodosh, and Julia Hockenmaier. From image descriptions to visual denotations: New similarity metrics for semantic inference over event descriptions. *Transactions of the association for computational linguistics*, 2:67–78, 2014.

Jiahui Yu, Yuanzhong Xu, Jing Yu Koh, Thang Luong, Gunjan Baid, Zirui Wang, Vijay Vasudevan, Alexander Ku, Yinfei Yang, Burcu Karagol Ayan, et al. Scaling autoregressive models for content-rich text-to-image generation. *arXiv preprint arXiv:2206.10789*, 2(3):5, 2022.

Sixian Zhang, Bohan Wang, Junqiang Wu, Yan Li, Tingting Gao, Di Zhang, and Zhongyuan Wang. Learning multi-dimensional human preference for text-to-image generation. In *Proceedings of the IEEE/CVF Conference on Computer Vision and Pattern Recognition*, pp. 8018–8027, 2024.

Ting Zhou, Daoyuan Chen, Qirui Jiao, Bolin Ding, Yaliang Li, and Ying Shen. Humanvbench: Exploring human-centric video understanding capabilities of mllms with synthetic benchmark data. *arXiv preprint arXiv:2412.17574*, 2024.

Deyao Zhu, Jun Chen, Xiaoqian Shen, Xiang Li, and Mohamed Elhoseiny. Minigpt-4: Enhancing vision-language understanding with advanced large language models. *arXiv preprint arXiv:2304.10592*, 2023.

Jinguo Zhu, Weiyun Wang, Zhe Chen, Zhaoyang Liu, Shenglong Ye, Lixin Gu, Hao Tian, Yuchen Duan, Weijie Su, Jie Shao, et al. Internvl3: Exploring advanced training and test-time recipes for open-source multimodal models. *arXiv preprint arXiv:2504.10479*, 2025.

Table of Contents

A Overview of the Appendix	16
B Spatial Partitioning Scheme	17
C Configurations of Evaluated Models	18
D Time Consumption and Resource Utilization	18
E LLM Prompt Design for Our Pipeline	19
F Evaluation Protocol	19
G Detailed Human Evaluation Results	21
H Mitigating the Impact of Inherent LLM Biases via Auxiliary Techniques	22
H.1 On Potential Bias in LLM-based Data Construction	22
H.2 On Potential Bias in LLM-based Evaluation	23
H.3 Experimental Validation	23
I Robustness of the Single-MLLM Evaluation Protocol	23
J Randomness Analysis for Evaluation with LLMs	24
K Compatibility of Our Framework with Other Evaluation Metrics	25
L Mini DETAILMASTER Benchmark	26
M Statistical Analysis of Metric Difficulty	26
N Negative Correlation between Prompt Length and Attribute Alignment	27
O Limitations	28
P Case Studies	29

A OVERVIEW OF THE APPENDIX

We provide more details and experiments of this work in the appendix and organize them as follows:

1. Core Methodology and Implementation Details:

- Appendix B, **Spatial Partitioning Scheme**: We present our Spatial Partitioning Scheme for categorizing bounding boxes into positional regions and validate its superior performance over the conventional nine-grid partitioning method.
- Appendix C, **Configurations of Evaluated Models**: We detail the configurations of all evaluated models, including image resolutions and key inference hyperparameters.
- Appendix D, **Time Consumption and Resource Utilization**: We document the computational costs associated with dataset construction and model evaluation, including detailed time consumption and GPU resource utilization.
- Appendix E, **LLM Prompt Design for Our Pipeline**: We detail the specific prompt designs employed throughout our LLM-driven pipeline. The effectiveness of our data construction and model evaluation stages relies heavily on these carefully crafted prompts, which are engineered to elicit precise and reliable outputs from the LLM.
- Appendix F, **Evaluation Protocol**: We provide a comprehensive technical specification of our evaluation pipeline, systematically detailing the methodologies employed to assess accuracy across four critical dimensions: “Character Attributes”, “Character Locations”, “Scene Attributes”, and “Entity Relationships”.

2. Robustness of Our Data Construction and Evaluation Protocol:

- Appendix G, **Detailed Human Evaluation Results**: We present detailed human evaluation results, validating our benchmark’s high reliability.
- Appendix H, **Mitigating the Impact of Inherent LLM Biases via Auxiliary Techniques**: We present an analysis of our pipeline against LLM-induced biases, empirically validating that our suite of auxiliary techniques ensures the objectivity and integrity of the data construction and evaluation protocol.
- Appendix I, **Robustness of the Single-MLLM Evaluation Protocol**: We present a robustness analysis of our LLM-based evaluation pipeline by re-running all evaluations with an alternative evaluator (InternVL3-9B). The results empirically demonstrate the robustness of our protocol: while a different evaluator may introduce score inflation, the relative model rankings and overarching analytical trends are preserved.
- Appendix J, **Randomness Analysis for Evaluation with LLMs**: We present a randomness analysis for our LLM-based evaluation pipeline, empirically confirming the reproducibility and robustness of our evaluation protocol through random seed experiments.

3. Supplementary Resources and Materials:

- Appendix K, **Compatibility of Our Framework with Other Evaluation Metrics**: We demonstrate the compatibility of our benchmark by empirically evaluating its outputs with established external metrics, confirming its utility as a specialized component within broader, multi-faceted evaluation pipelines.
- Appendix L, **Mini DETAILMASTER Benchmark**: We introduce a mini-benchmark (800 detail-rich long prompts) that maintains evaluation consistency with the full benchmark while significantly reducing resource requirements, enabling rapid model assessment.

4. Further Analysis and Insights:

- Appendix M, **Statistical Analysis of Metric Difficulty**: we present a systematic analysis of metric difficulty, quantitatively establishing a clear hierarchy from Character Locations (most difficult) to Scene Attributes (easiest). Furthermore, our qualitative investigation of failure cases reveals common error patterns that illuminate the underlying weaknesses of the models.

- Appendix N, **Negative Correlation between Prompt Length and Attribute Alignment**: We present the correlation analysis between prompt length and attribute accuracy in generated characters, demonstrating a consistent negative relationship between prompt length and attribute alignment fidelity.
- Appendix O, **Limitations**: We examine the limitations of our work, specifically addressing constraints in both the characteristics of our evaluation data and evaluation pipeline.
- Appendix P, **Case Studies**: We present representative case studies, and validate the accuracy of our comparative evaluations in the main text.

B SPATIAL PARTITIONING SCHEME

In this section, we introduce our Spatial Partitioning Scheme, a method employed in the attribute extraction pipeline to categorize bounding boxes into approximate positional regions (e.g., “the upper part of the image”). This strategy is introduced because, in practical use, raw bounding box coordinates are typically excluded from prompts in favor of positional descriptions.

To maximize the extraction of character location features, we deviate from the conventional 3×3 grid partitioning, as we observe that characters often lie near region boundaries, making region classification difficult. Instead, we introduce slight overlaps between adjacent regions by expanding their boundaries, increasing the likelihood of larger character area coverage within a given region. This adjustment enhances the assignment of positional labels, ultimately enriching the extracted “Character Locations” features and resulting in prompts with more character location information. (Notably, this partitioning scheme is applied exclusively during attribute extraction to augment both the quantity and balance of “Character Locations” data. However, during evaluation, we do not apply this scheme and directly assess positional accuracy by comparing bounding boxes against prompt specifications using the MLLM to ensure precise measurement.)

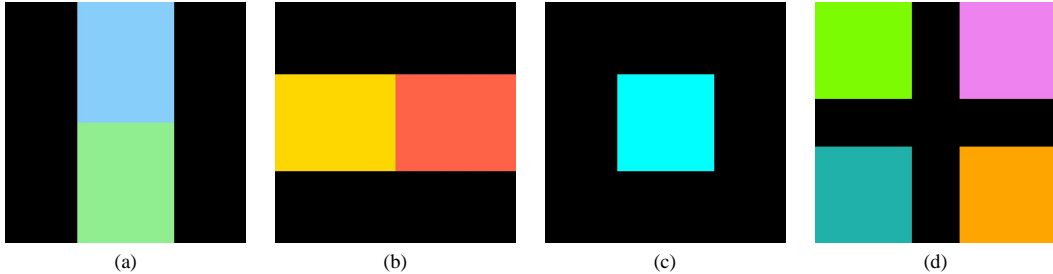


Figure 4: The visualization of the nine grids: (a) shows the upper part and the lower part; (b) shows the left part and the right part; (c) shows the middle part; while (d) shows all four corner regions: the upper left part, the lower left part, the upper right part, and the lower right part.

Our spatial partitioning scheme defines nine distinct regions within a normalized 1×1 coordinate space, where each region is represented as $[x_0, y_0, x_1, y_1]$ with (x_0, y_0) denoting the top-left coordinates and (x_1, y_1) denoting the bottom-right coordinates. Specifically, we define: the upper part as $[0.3, 0, 0.7, 0.5]$, the lower part as $[0.3, 0.5, 0.7, 1]$, the left part as $[0, 0.3, 0.5, 0.7]$, the right part as $[0.5, 0.3, 1, 0.7]$, and the middle part as $[0.3, 0.3, 0.7, 0.7]$. Additionally, we establish four corner regions: the upper left $[0, 0, 0.4, 0.4]$, lower left $[0, 0.6, 0.4, 1]$, upper right $[0.6, 0, 1, 0.4]$, and lower right $[0.6, 0.6, 1, 1]$. As illustrated in Figure 4, this partitioning scheme provides systematic coverage of the image space while maintaining clear semantic correspondence with spatial relationships. With the nine regions, we first normalize the character’s bounding box coordinates, then calculate the proportional area overlap between the normalized box and each of the nine spatial regions. The final position classification is determined by selecting the region that covers at least 75% of the character’s bounding box area and shows the highest proportional overlap among all qualifying regions. For cases where no region meets the 75% coverage threshold (indicating boundary straddling), we assign a “null” location designation.

To validate the effectiveness of our partitioning scheme, we conduct a comparative analysis between the conventional 3×3 grid method and our proposed scheme by examining the proportion of

Table 4: Compared with the conventional 3×3 grid method, our partitioning scheme extracts richer valid character location labels and maintains matching accuracy with actual character locations.

	Proportion of “null” Character Location Labels	Matching Rate Between Labels and Actual Locations
Conventional 3×3 Grid Method	66.19%	95.91%
Our Partitioning Scheme	32.68%	95.52%

ambiguous character positions (marked as “null”) at region boundaries. The experimental results show: while the traditional method classify 7,821 out of 11,816 characters (66.19%) as “null” due to boundary ambiguity, our partitioning scheme reduce this number to only 3,862 (32.68%). This reduction provides empirical evidence that our scheme effectively prevents characters from being situated near region boundaries and extracts more valid positional descriptions.

Additionally, we employ the MLLM Qwen2.5-VL-7B-Instruct to verify the consistency between our position descriptions and actual character locations, following the same method as our evaluation pipeline: we highlight characters with red bounding boxes and provide both the box coordinates and the position descriptions to the MLLM for verification. Comparative analysis reveal that while the conventional 3×3 grid method achieved 95.91% accuracy, our proposed method attain 95.52% accuracy. This marginal difference shows that our scheme successfully maintains comparable localization accuracy while significantly increasing the number of detectable character positions, confirming that our partitioning strategy achieves an optimal balance between precision and coverage.

C CONFIGURATIONS OF EVALUATED MODELS

In this section, we detail the configurations for image generation across different models in our evaluation. Regarding the output resolution, we adopt 512×512 pixels for SD1.5 and its derivative models to align with their training settings, while setting 1024×1024 pixels for all other models. For inference steps (num_inference_steps), we follow each model’s reference implementations: 100 steps for DeepFloyd IF and ParaDiffusion, 70 steps for ELLA, and 50 steps for remaining models. The guidance scale parameters are similarly configured according to official recommendations: 11 for ELLA, 7 for DeepFloyd IF, 5 for SD-XL, 3.5 for both FLUX and SD3.5, and 7.5 for all other models.

Regarding the two proprietary models, Gemini 2.0 Flash and GPT Image-1, we access their official APIs, specifically “gemini-2.0-flash-exp-image-generation” and “gpt-image-1” respectively, setting the default hyperparameters for image generation.

For LLM Blueprint, we employ Qwen2.5-7B-Instruct as the LLM to perform attribute extraction and position extraction from long prompts. For Deepfloyd IF, “IF-I-XL-v1.0” serves as the first-stage model, “IF-II-L-v1.0” serves as the second-stage model, and “stable-diffusion-x4-upscaler” serves as the upscaler.

For the long-prompt optimized models, we employ the highest-performing open-source backbones available for each model. It should be noted that while superior backbones have been described in their papers, their unavailability in open-source repositories precludes their inclusion in our evaluations.

D TIME CONSUMPTION AND RESOURCE UTILIZATION

In this section, we present the computational requirements of our data construction pipeline and evaluation pipeline.

For the first stage of our data construction pipeline (using Qwen2.5-VL-7B-Instruct and Qwen2.5-14B-Instruct), processing 164K detailed captions to produce 4,565 refined prompts on a single NVIDIA L20 GPU requires: 55 hours for “Main character identification”, 24 hours for “Character localization”, 77 hours for “Character attribute extraction”, 36 hours for “Scene attribute and entity relationship detection”, 55 hours for “Prompt refinement”, and 59 hours for “Prompt filtering”.

For the second stage of our data construction pipeline (i.e. “Prompt enhancement” with Qwen2.5-VL-72B-Instruct), processing 4,565 prompts derived from the first stage to produce 4,116 final pol-

ished prompts using 8 NVIDIA L20 GPUs requires: 3.3 hours for “Main character identification”, 6 hours for “Character localization”, 27.4 hours for “Character attribute extraction”, 12.9 hours for “Scene attribute and entity relationship detection”, 22.6 hours for “Prompt refinement”, and 22.2 hours for “Prompt filtering”.

The evaluation pipeline typically consumes 10 hours using a single NVIDIA L20 GPU, with duration positively correlated with the quality of generated images.

Regarding the GPU memory, both our data construction pipeline’s first stage and the evaluation pipeline require 20GB-39GB of GPU memory. When executing the second stage of our data construction pipeline across 8 GPUs, each GPU shows memory usage ranging from 26GB to 38GB. The variation in memory requirement arises due to the different values of the “cache_max_entry_count” parameter, ranging from 0.01 to 0.8. Additionally, the previously reported time consumption is measured with the “cache_max_entry_count” parameter set to 0.8.

E LLM PROMPT DESIGN FOR OUR PIPELINE

In this section, we present the prompt designs for the LLMs (MLLMs) used in our data construction and model evaluation phases.

In the “Main Character Identification” stage of our data construction process, we employ a few-shot approach to construct prompts that guide the model to respond in a JSON format. The prompt informs the model that it will be provided with “*an image and its corresponding description*”, and its task is to “*identify and count the main characters in the image*”. During prompt tuning, we experimented with zero-shot prompting but observed unsatisfactory performance. We also tried omitting the character count, which similarly degraded results.

For the “Character Localization” stage, we use the prompt “*Please only provide the bounding box coordinates of the region CHARACTER describes*”, where CHARACTER refers to the identified main character from the previous stage. While Qwen2.5-VL-Instruct generally adheres to this instruction, occasional localization errors lead us to deploy an open-set detector YOLOE-11L to vote for the correct bounding box coordinates.

When extracting character attributes, we provide the model with the relevant image captions and, when necessary, highlight or crop the target regions of the characters while also supplying examples of the attributes to be extracted. During prompt tuning, we evaluated two alternative approaches: one eliminating image captions and another removing cropping/highlighting operations. Both configurations resulted in fewer extracted attributes.

In the “Prompt Refinement” stage, we iteratively refine the image captions by prompting the model to supplement missing attributes: “*Some of the CATEGORY attribute information in the image description is missing. Your task is to supplement the missing CATEGORY attribute information into the image description.*” Here, CATEGORY denotes different attribute types. For the “Filtering” stage, we prompt the model to determine which attributes are absent from the caption: “*Your task is to determine whether the given image description includes the description of this particular CATEGORY feature of the main character.*”

For evaluating “Character Attribute”, we prompt the MLLM to analyze each attribute individually, using cropped images of the characters: “*Please analyze the main character in this image, specifically the CHARACTER. Please determine whether ATTRIBUTE is one of its characteristics or is associated with it.*” Here, CHARACTER and ATTRIBUTE are the specific character name and the attribute being evaluated. In the “Character Location” evaluation, we highlight the image and provide positional coordinates, prompting the MLLM to assess whether the object’s location matches the reference. Regarding the feature evaluation for the entire image, the MLLM directly judges based on the image content and attribute categories.

F EVALUATION PROTOCOL

We design a multi-stage evaluation pipeline to rigorously assess compositional text-to-image generation. The pipeline initiates by instructing text-to-image models with prompts from **DETAIL-MASTER** to produce corresponding image sets, followed by automated main character detection

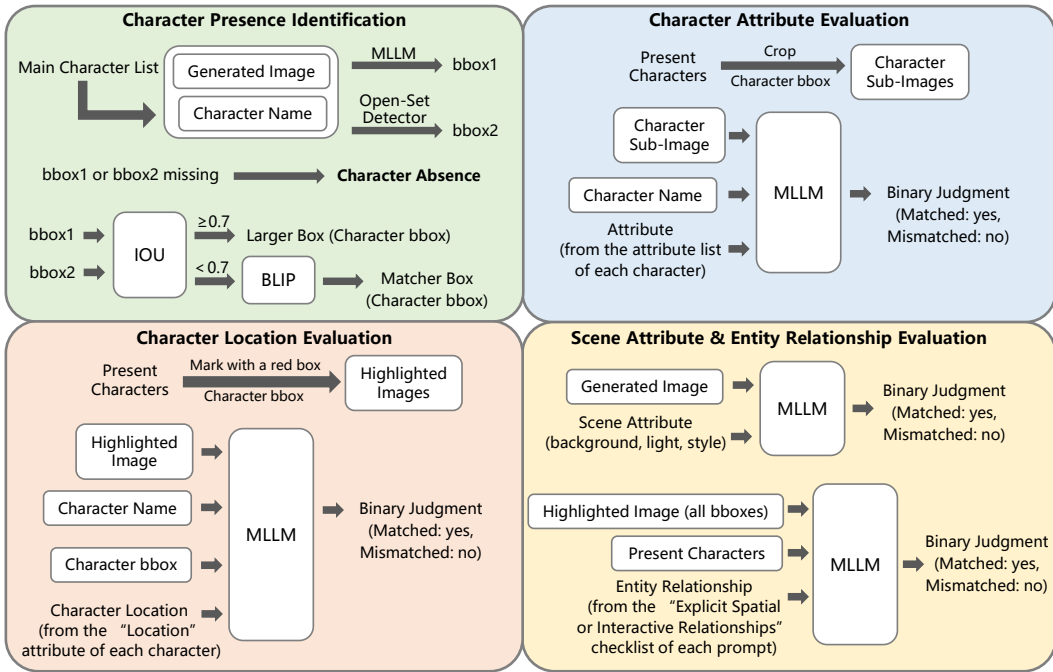


Figure 5: Overview diagram of the evaluation pipeline for the **DETAILMASTER** benchmark.

and localization within the images. Subsequently, we perform sequential evaluations across four critical dimensions: 1) “Character Attributes”, 2) “Character Locations”, 3) “Scene Attributes”, and 4) “Entity Relationships”. Regarding the evaluator, we employ Qwen2.5-VL-7B-Instruct as the MLLM throughout the evaluation process.

This section provides comprehensive technical specifications of our evaluation pipeline, detailing the methodologies and validation mechanisms implemented for each evaluation dimensions.

Character presence identification. Initially, we implement a dual-model verification system for character detection, where a character is deemed successfully generated only if its presence is confirmed by both an MLLM and the YOLOE-11L open-set detector. For the confirmed characters, we also record their box coordinates to assist the subsequent attribute evaluation. Regarding how to determine the box coordinates, we calculate the IoU score between the two bounding boxes detected. If the score exceeds 0.7, we consider the boxes as overlapping and select the larger bounding box. Otherwise, we employ the vision-language model BLIP to compute image-text matching scores between both bounding box regions and the character name, selecting the box with a higher score. Identifying character presence can accelerate the whole evaluation process by eliminating redundant computations for failed generations. And it also avoids repetitive detection steps as the positional information can be reused.

“Character Attribute” evaluation. Our methodology for character attribute evaluation involves three main steps. First, we crop sub-images of individual present characters using their positional information. Second, each sub-image is processed by an MLLM, which renders a binary (“yes” or “no”) judgment on the presence of each specified attribute. Third, we measure performance by calculating the accuracy of attribute generation. This metric is computed separately for objects, animals, and persons to allow for a detailed, category-level performance analysis.

“Character Location” evaluation. For character location evaluation, we sequentially process each identified character and mark its position in the generated image with a red bounding box. The bounding box information are then provided to the MLLM along with explicit instructions that the red box marks the target character. And the MLLM is prompted to determine whether the character location precisely aligns with the position description, responding with a yes/no judgment. The

final character location accuracy is calculated as the proportion of correctly positioned characters to the total number of characters who have “Character Location” attribute.

“Scene Attribute” evaluation & “Entity Relationship” evaluation. For scene attribute evaluation, we ask the MLLM to determine whether the generated images satisfy each specified “Scene Attribute” with yes/no responses. The accuracy rates are calculated separately for background, lighting, and style attributes. Regarding entity relationship evaluation, for each generated image, we first mark all identified characters in the image with red bounding boxes. We then provide the MLLM with the marked image and the list of identified characters, and subsequently ask it to evaluate each attribute in the “Spatial/Interactive Relationships” checklist, determining whether the specified entity relationship aligns with the image content.

G DETAILED HUMAN EVALUATION RESULTS

In this section, we provide the details of our human evaluation on **DETAILMASTER**, expanding the three metrics introduced in the main text (Task Relevance, Source Image Fidelity, and Prompt Consistency). Specifically, we systematically examine our benchmark based on the four key generation tasks.

Table 5: Human evaluation details for “Character Attributes”.

Category	Categorical Verification	Presence Confirmation	Prompt Inclusion	Attribute-Image Alignment	Attribute-Prompt Completeness
Object	100%	100%	100%	96.21%	97.64%
Animal	100%	99%	100%	98.22%	98.22%
Person	100%	98%	99%	91.58%	96.17%

For the “Character Attributes” (encompassing “object”, “animal”, and “person” categories), our annotators conduct a five-component examination for each designated main character: 1) **Categorical Verification** - determining whether the character correctly aligns with the annotated category; 2) **Presence Confirmation** - determining whether the character is in the source image; 3) **Prompt Inclusion** - determining whether the character is explicitly mentioned in the final polished prompt; 4) **Attribute-Image Alignment** - quantifying the proportion of annotated attributes that accurately align with the source image; and 5) **Attribute-Prompt Completeness** - quantifying the proportion of annotated attributes that are explicitly described in the final prompt. The results are shown in Table 5.

Table 6: Human evaluation details for “Character Locations”.

Presence Confirmation	Bounding Box Containment	Positional Accuracy	Prompt Inclusion
100%	99%	100%	99%

For the “Character Locations”, we employ a four-component spatial verification process: 1) **Presence Confirmation** - determining whether the character is in the source image; 2) **Bounding Box Containment** - determining whether the character falls in our annotated bounding box region (visually highlighted with a red rectangle); 3) **Positional Accuracy** - comparing the character’s actual placement against our position annotations (e.g., “the upper left part of the image”); and 4) **Prompt Inclusion** - checking whether the spatial information in the final prompt matches our position annotations. The results are shown in Table 6.

Table 7: Human evaluation details for “Scene Attributes”.

Category	Categorical Verification	Scene.Attribute-Image Alignment	Prompt Inclusion
Background	100%	99%	100%
Light	100%	91%	99%
Style	100%	100%	100%

For the “Scene Attributes” (covering background, lighting, and style conditions), we involve three systematic checks: 1) **Categorical Verification** - validating that the annotated “scene_attribute_content” correctly describes the annotated visual condition (i.e., background,

lighting, and style); 2) **Scene_Attribute-Image Alignment** - determining whether the annotated “scene_attribute_content” aligns with the source image; and 3) **Prompt Inclusion** - determining whether the annotated “scene_attribute_content” is unambiguously specified in the final prompt. The results are shown in Table 7.

Table 8: Human evaluation details for “Entity Relationships”.

Entity_Relationship-Image Alignment	Entity_Relationship-Prompt Completeness
88.58%	97.89%

For the “Entity Relationship”, we focus on two critical aspects: (a) **Entity_Relationship-Image Alignment** - quantifying the proportion of annotated entity relationships that correctly align with the source image; and (b) **Entity_Relationship-Prompt Completeness** - quantifying the proportion of annotated entity relationships that are explicitly described in the final prompt. The results are shown in Table 8.

As shown in the human evaluation results, the evaluation data of our benchmark achieves near-perfect performance across all metrics, with most scores approaching 100%, confirming the high standard of our attribute extraction pipeline. However, a few metrics exhibit relatively lower scores, such as the Attribute-Image Alignment for the “Person” category in “Character Attributes” (91.58%), the Scene_Attribute-Image Alignment for the “Light” category in “Scene Attributes” (91%), and the Entity_Relationship-Image Alignment in “Entity Relationships” (88.58%). Notably, these metrics all pertain to the alignment between annotated features and the source images, and their failure to reach full scores suggests a few instances of hallucination during attribute extraction. Nevertheless, the corresponding “Prompt Inclusion” and “Prompt Completeness” metrics for these features consistently approach 100%, indicating that while rare discrepancies may occur between annotations and visual content, these features are still incorporated into the final prompts. This ensures that the evaluation accuracy remains largely unaffected, as the prompt-conditional generation faithfully reflects the annotated features rather than the features in the source images.

H MITIGATING THE IMPACT OF INHERENT LLM BIASES VIA AUXILIARY TECHNIQUES

Our pipeline leverages advanced LLMs for data construction and model evaluation. A critical consideration, therefore, is the potential influence of inherent biases from these models. In this section, we address this concern and present supplementary experiments to demonstrate that our pipeline is robust against such biases. We argue that the extensive integration of auxiliary techniques at each stage effectively mitigates these potential influences, ensuring the quality and objectivity of our dataset and evaluation process.

H.1 ON POTENTIAL BIAS IN LLM-BASED DATA CONSTRUCTION

A primary concern is that sole reliance on LLMs for data generation could introduce inherent biases of the models. To counteract this, we integrate a suite of auxiliary techniques into our data construction workflow, including open-set object detection, image cropping, image highlighting, and few-shot prompting. These techniques serve to ground the MLLM’s outputs in objective image features rather than learned priors, enhancing the accuracy and diversity of the generated data. This multi-faceted approach ensures that our dataset is not exclusively dependent on the generative capabilities of any single LLM, thereby insulating it from model-specific biases.

Furthermore, our selection of MLLM is also a deliberate step in quality control. We benchmark three leading models—Qwen2.5-VL-Instruct, InternVL2.5 (Chen et al., 2024), and LLaVA-OneVision (Li et al., 2024b)—and observe that Qwen2.5-VL-Instruct exhibits more rigorous logical reasoning and generates more precise outputs. Consequently, we select it as the primary MLLM for our data construction pipeline.

H.2 ON POTENTIAL BIAS IN LLM-BASED EVALUATION

A second concern is a potential evaluation bias favoring text-to-image models that use LLM-based text encoders, given that our data is constructed with LLMs. This concern is unfounded for two main reasons. First, the LLMs employed as text encoders in the evaluated models (e.g., Llama-2, T5-XL) are architecturally distinct and typically older than the LLM chosen for our data construction, Qwen2.5-VL-Instruct. (For the LLM Blueprint model specifically, while we employ Qwen2.5-7B-Instruct for object name extraction from prompts, this LLM functions only as a pre-processing component and is not the text encoder used during image generation.)

Second, as previously detailed, our extensive use of auxiliary techniques ensures the rich diversity and factual accuracy of our **DETAILMASTER** dataset. This effectively decouples the dataset from an over-reliance on the specific characteristics of Qwen2.5-VL-Instruct, minimizing the potential inherent biases that could favor a particular model architecture during evaluation.

H.3 EXPERIMENTAL VALIDATION

To empirically validate our claims, we conduct additional ablation studies analyzing the impact of our auxiliary techniques and the choice of LLMs on the data construction process.

Impact of auxiliary techniques on data quality. We first examine the effect of the deployed open-set object detector during the Character Localization stage. Our findings indicate that this step corrects 16.6% of bounding box coordinates proposed by the MLLM, enhancing localization accuracy.

Next, we investigate the consequences of omitting image cropping during the Character Attribute Extraction stage. Specifically, we employ Gemini-2.5-Flash (Comanici et al., 2025) to evaluate the accuracy of each generated annotation. While the accuracy remains relatively stable, we observe a 15.1% reduction in the number of extracted attributes. This demonstrates that our image cropping is crucial for enabling the MLLM to perform a more comprehensive and detailed analysis.

Impact of MLLM choice on data generation. As previously mentioned, Qwen2.5-VL-Instruct shows relatively strict inference behavior, which our new experiment further confirms. We replicate the Character Attribute Extraction pipeline using InternVL3-9B (Zhu et al., 2025) and evaluate the resulting annotations with Gemini-2.5-Flash. The results indicate a 3.4% decrease in accuracy. Moreover, due to format errors in InternVL3-9B’s outputs (e.g., failure to adhere to list format), the quantity of generated attributes decreases by 24.5%.

In conclusion, this section has rigorously addressed the critical issue of LLM-induced bias within our pipeline. Through a series of targeted experiments, we have demonstrated conclusively that our suite of auxiliary techniques is indispensable for achieving high data quality. These methods not only rectify potential inaccuracies but also enrich the detail of our generated data. The performance degradation observed when substituting our carefully selected MLLM further underscores the efficacy of our overall approach. Therefore, we assert with confidence that our pipeline is robust against LLM-specific biases, establishing the **DETAILMASTER** dataset as a reliable and impartial resource for the community.

I ROBUSTNESS OF THE SINGLE-MLLM EVALUATION PROTOCOL

It is a common practice in existing benchmarks for text-to-image models to employ a single MLLM for evaluation. For instance, T2I-CompBench utilizes only Minigpt-4 (Zhu et al., 2023) for feature verification, while DPG-Bench relies on a single mPLUG-large model (Li et al., 2022a) for characteristic assessment. There are two primary reasons why benchmark works typically deploy only a single MLLM: (1) Deploying multiple MLLMs consumes significant time and GPU computing resource; (2) Adapting prompts, auxiliary tools, or evaluation frameworks for different MLLMs would lead to overly cumbersome inference code.

Actually, our selection of Qwen2.5-VL-7B-Instruct is based on comparisons. We evaluate it against InternVL2.5 (Chen et al., 2024) and LLaVA-OneVision(Li et al., 2024b), and find that Qwen2.5-VL-7B-Instruct demonstrates stricter judgment criteria. It shows superior accuracy in identifying

object features while exhibiting strong adherence to prescribed output formats. In contrast, both InternVL2.5 and LLaVA-OneVision exhibit a tendency to respond “yes” more readily during feature evaluation, which consequently leads to inflated scores.

We conduct a new set of experiments, re-running our entire evaluation pipeline using InternVL3-9B. The results are presented in Table 9.

Table 9: Evaluation results on the **DETAILMASTER** Benchmark (with InternVL3-9B).

Model	Character Attributes			Character Locations	Scene Attributes			Entity Relationships
	Object	Animal	Person		Background	Light	Style	
SD1.5	22.62	24.03	17.84	11.90	33.48	77.20	83.90	12.99
SD-XL	36.41	44.03	29.19	20.97	38.62	79.82	69.65	19.63
DeepFloyd IF	54.75	57.92	45.25	33.11	37.12	79.66	85.18	28.30
SD3.5 Large	67.57	78.99	55.38	59.26	95.66	95.11	96.28	67.18
FLUX.1-dev	71.42	79.42	55.61	67.13	98.85	98.78	96.01	74.41
Gemini 2.0 Flash	72.37	80.08	54.65	69.31	98.72	98.62	97.51	77.27
GPT Image-1	73.44	83.81	59.02	69.95	99.51	99.11	95.75	82.51
LLM4GEN	24.25	30.76	21.13	14.66	35.82	77.86	55.06	16.23
LLM Blueprint	22.02	22.90	18.65	28.26	66.03	87.79	65.30	20.61
ELLA	41.92	49.76	34.93	27.99	57.82	84.44	42.66	26.74
LongAlign	40.54	47.52	26.53	25.98	86.26	93.00	84.58	31.61
ParaDiffusion	51.68	52.84	39.11	45.88	90.45	95.45	68.13	56.88

As shown in the table, with InternVL3-9B, all models show varying degrees of score improvement. This observation aligns with our previous experimental findings on InternVL2.5, suggesting that using InternVL3-9B for evaluation is not sufficiently rigorous, as it tends to favor “yes” responses when assessing ambiguous features.

However, despite the overall score improvement, the comparative rankings among the models and the general score trends remain unchanged. For general-purpose T2I models, more advanced models consistently achieve higher scores. Similarly, long-prompt optimized T2I models outperform the baseline models SD1.5 and SD-XL.

Regarding additional details, for instance:

- Top-tier proprietary models (GPT Image-1, Gemini 2.0 Flash) still outperform all other models, with more advanced models consistently achieving higher scores.
- Long-prompt-specific models (ParaDiffusion, LongAlign, ELLA) still show clear advantages over baselines like SD-XL on complex attributes.
- ParaDiffusion continues to excel in Character Locations and Entity Relationships compared to other long-prompt-specific models, validating the effectiveness of task-specific adaptive training (Jiao et al., 2024; Xu et al., 2025).
- We also compute the Kendall’s Tau Correlation Coefficient between the evaluation results obtained with the two MLLMs. The correlation coefficients for each metric are as follows: 0.879, 0.909, 0.909, 0.909, 0.970, 1.000, 0.879, and 0.970. These consistently high values (all approaching 1.0) reflect a strong positive correlation between the two MLLM evaluators, confirming the consistent scoring trends across the evaluated models.

This cross-evaluator consistency provides strong evidence that our benchmark’s conclusions are robust and not an artifact of the specific MLLM used.

J RANDOMNESS ANALYSIS FOR EVALUATION WITH LLMs

To assess the impact of randomness inherent in LLM-based evaluation, we conduct experiments by varying random seeds and setting the LLM temperature to 0.8, subsequently repeating evaluation across five representative models (SD1.5, LongAlign, LLM Blueprint, FLUX.1-dev, and GPT Image-1) to quantify stochastic variability. The results are shown in 10.

The presented results show that the randomness introduced by LLMs in our evaluation framework has minimal impact, with repeated assessments across all models showing negligible variations (Δ

Table 10: Robustness evaluation of LLM-based assessment randomness.

Model	Character Attributes			Character Locations	Scene Attributes			Spatial Attributes
	Object	Animal	Person		Background	Light	Style	
FLUX.1-dev (1)	51.47	45.83	34.91	41.57	95.77	97.05	94.81	47.49
FLUX.1-dev (2)	51.72	45.89	35.60	41.57	95.77	97.05	94.81	47.49
FLUX.1-dev (3)	51.53	45.85	34.97	41.57	95.77	97.05	94.81	47.45
GPT Image-1 (1)	59.47	48.12	40.43	53.93	97.50	98.85	97.69	63.03
GPT Image-1 (2)	59.47	48.12	40.43	53.93	97.50	98.85	97.69	63.03
GPT Image-1 (3)	59.47	48.12	40.43	53.93	97.50	98.85	97.69	63.03
LLM Blueprint (1)	21.41	27.01	13.91	18.44	50.89	77.57	64.24	11.60
LLM Blueprint (2)	21.42	26.97	13.85	18.46	50.89	77.57	64.24	11.65
LLM Blueprint (3)	21.32	26.97	13.67	18.46	50.89	77.57	64.24	11.62
LongAlign (1)	32.95	34.60	15.35	14.89	77.03	87.70	72.27	19.17
LongAlign (2)	32.95	34.60	15.35	14.89	77.03	87.70	72.27	19.09
LongAlign (3)	32.99	34.56	15.38	14.92	77.03	87.70	72.27	19.11
SD1.5 (1)	20.79	27.69	13.89	8.68	22.02	64.52	80.90	5.88
SD1.5 (2)	20.76	27.68	13.92	8.68	22.02	64.52	80.90	5.84
SD1.5 (3)	20.78	27.62	13.93	8.68	22.02	64.52	80.90	5.84

$< 0.5\%$). This robust consistency strongly validates the stability and reliability of our evaluation protocol, ensuring reproducible and dependable model comparisons regardless of inherent LLM randomization factors.

K COMPATIBILITY OF OUR FRAMEWORK WITH OTHER EVALUATION METRICS

Our work specifically focuses on the adherence of T2I models to detailed, long prompts. Consequently, metrics such as “visual quality” and “safety” fall outside the scope of our objectives. Nevertheless, our benchmark is fully compatible with other frameworks that assess “visual quality” and “safety” scores. The prompts and generated images from our dataset can be readily integrated into such frameworks to obtain these corresponding scores.

To demonstrate this compatibility, we evaluate our prompts and generated images using several established external metrics: (1) DiffSynth-Studio’s ImageReward (for image quality), Aesthetic (for aesthetic scores), and HPSv2.1 and MPS (for human preference scores) (Xu et al., 2023; Duan et al., 2024; Wu et al., 2023b; Zhang et al., 2024); and (2) Falcons-ai’s nsfw_image_detection (for safety assessment) (Falcons.ai, 2023).

Table 11: Demonstration of compatibility with external evaluation frameworks.

Model	ImageReward	Aesthetic	HPSv2.1	MPS	nsfw_image_detection
SD-XL	0.08	5.67	0.2831	9.69	0.0011
FLUX.1-dev	0.45	5.41	0.2921	9.89	0.0005
ELLA	0.23	5.52	0.2486	9.18	0.0021
ParaDiffusion	0.16	5.60	0.2733	8.48	0.0011

As shown in Table 11, our benchmark can be effectively combined with other evaluation frameworks to obtain other metrics. In our code repository, we will include hyperlinks to these external evaluation frameworks, providing users with the flexibility to choose additional metrics according to their specific needs.

Furthermore, the method’s ability to extract fine-grained information from individual image entities makes it a powerful tool for constructing datasets and benchmarks for guided data-model co-development (Qin et al., 2025). Applications include discerning subtle differences between similar images (Jiao et al., 2025), capturing nuanced human attributes like actions and expressions (Zhou et al., 2024), generating Visual Question Answering (VQA) samples (Kuang et al., 2025b), and annotating unconventional data types, such as images containing emojis or web GUIs (Kuang et al., 2025a; Luo et al., 2025).

L MINI DETAILMASTER BENCHMARK

To address computational resource constraints and facilitate rapid evaluation for researchers, we develop a mini version of our **DETAILMASTER** benchmark comprising 800 detail-rich long prompts. The construction methodology for the mini benchmark employs a sampling approach across four key dimensions: 1) For “Character Attributes”, we analyze the distribution of object, animal, and person entities in each sample, selecting candidates containing more than two instances of each category into respective attribute candidate pools (i.e., “Object Attributes”, “Animal Attributes”, “Person Attributes”); 2) For “Character Locations”, samples featuring more than three localizable characters are included in the location candidate pool; 3) For “Scene Attributes”, candidates are selected based on the presence of background descriptions, lighting conditions, or style specifications (i.e., “Background Attributes”, “Lighting Attributes”, “Style Attributes”); 4) For “Entity Relationships”, samples are filtered by requiring a minimum of five spatial or interactive relationships. The final mini benchmark composition is achieved through balanced random sampling, extracting 100 prompts from each of these eight candidate pools to form a representative yet efficient evaluation set. We conduct a comprehensive reevaluation of all 12 models discussed in the main text using our mini **DETAILMASTER** benchmark, with the comparative results presented in Table 12.

Table 12: Evaluation results on the **mini DETAILMASTER** Benchmark. All values in the table represent accuracy percentages.

Model	Backbone	(A) General-Purpose Text-to-Image Model								
		Character Attributes			Character Locations	Scene Attributes			Spatial Attributes	
		Object	Animal	Person		Background	Light	Style		
SD1.5	-	14.76	21.81	9.85	7.11	20.11	65.62	85.94	6.03	
SD-XL	-	18.48	21.92	11.58	10.87	26.36	69.01	70.05	8.22	
DeepFloyd	-	22.40	23.85	20.77	14.72	24.52	68.23	86.98	12.60	
SD3.5 Large	-	36.36	32.27	23.00	35.45	94.57	88.80	98.70	35.99	
FLUX.1-dev	-	37.90	38.57	27.43	46.66	97.83	97.14	95.83	43.04	
Gemini 2.0 Flash	-	47.21	36.82	27.14	46.15	97.67	96.88	98.91	46.35	
GPT Image-1	-	50.96	39.42	31.23	66.06	98.75	98.84	95.40	55.87	

Model	Backbone	(B) Long-Prompt Optimized Text-to-Image Model								
		Character Attributes			Character Locations	Scene Attributes			Spatial Attributes	
		Object	Animal	Person		Background	Light	Style		
LLM4GEN	SD1.5	16.47	23.84	15.48	7.53	23.64	67.71	51.56	6.30	
LLM Blueprint	SD1.5	15.57	23.51	14.29	17.93	54.46	76.67	53.03	10.40	
ELLA	SD1.5	28.09	24.96	16.64	14.46	51.36	68.75	36.20	12.13	
LongAlign	SD1.5	26.08	23.42	13.91	15.97	85.60	81.25	63.80	15.45	
ParaDiffusion	SDXL	28.97	28.40	17.51	18.56	89.40	88.80	60.36	18.66	

The comparative results in Table 12 show that the performance comparison and trends across models remain consistent between our **mini DETAILMASTER** benchmark and the full **DETAILMASTER** benchmark. As the mini benchmark contains more challenging samples selected for their greater detail complexity, the scores on the mini benchmark are generally lower than those on the full version. Crucially, the preserved consistency combined with improved evaluation efficiency enables researchers to more effectively assess model performance in handling long prompts. Therefore, the mini benchmark serves as an efficient alternative for resource-constrained scenarios or time-sensitive evaluations, while maintaining comparable validity to the full benchmark.

M STATISTICAL ANALYSIS OF METRIC DIFFICULTY

In this section, we present an experimental analysis of the relative difficulty of our four metrics. Furthermore, we conduct a failure case analysis to investigate instances where the evaluated models perform inaccurately.

Specifically, for each sample, we calculate the proportion of correctly generated attributes for each evaluation metric. If a model achieves a correct proportion below 50% for a specific metric, we consider that metric hard for the model on that sample (e.g., if a sample’s prompt contains eight “animal attributes” and the model generates fewer than four correct “animal attributes”, we consider the “Animal” generation task hard for the model on that sample).

The evaluation metrics we examine include: “Object”, “Animal”, “Person”, “Character Locations”, “Scene Attributes”, and “Entity Relationships”. Notably, the “Character Attributes” metric in our main evaluation is split into “Object”, “Animal”, and “Person” for individual analysis. Meanwhile, the sub-metrics of “Scene Attributes” (i.e., “Background”, “Light”, and “Style”) are aggregated.

The results present the proportion of hard samples for each metric. We also calculate the average value across all evaluated models, as presented in the “Average” row. The final outcomes are shown in Table 13.

Table 13: Proportion of hard samples for each metric.

Model	Character Attributes			Character Locations	Scene Attributes	Entity Relationships
	Object	Animal	Person			
SD1.5	82.6%	75.7%	88.2%	95.8%	38.6%	98.1%
SD-XL	79.0%	74.0%	85.2%	94.2%	40.8%	95.7%
DeepFloyd IF	72.1%	64.8%	77.1%	92.3%	33.3%	94.6%
SD3.5 Large	54.4%	56.0%	69.6%	76.5%	2.7%	62.9%
FLUX.1-dev	51.7%	56.5%	67.9%	68.8%	0.8%	52.2%
Gemini 2.0 Flash	47.1%	56.2%	68.9%	65.8%	0.6%	47.4%
GPT Image-1	42.7%	55.6%	62.9%	55.2%	0.2%	32.4%
LLM4GEN	81.7%	73.8%	84.9%	95.3%	52.8%	97.3%
LLM Blueprint	82.0%	74.5%	87.8%	88.3%	29.4%	94.5%
ELLA	69.0%	68.5%	79.9%	90.9%	43.6%	90.4%
LongAlign	71.2%	68.1%	86.4%	91.9%	11.6%	87.0%
ParaDiffusion	68.3%	68.6%	80.1%	88.1%	9.8%	80.0%
Average	66.8%	66.0%	78.2%	83.6%	22.0%	77.7%

As shown in the table, the most challenging metric is “Character Locations”. We check cases where all models made errors on this metric and identify two main reasons for the failures: (1) The object positions described in the prompt may contradict conventional real-world positions in photos. For instance, when the prompt states that traffic lights are in the “lower part” of the image while they typically appear in the “upper part” in real photos, this discrepancy leads to positional misalignment. (2) The models exhibit a tendency to generate objects in the middle of the image, even when the prompt specifies left or right placement.

The second most challenging metric is “Person” under the “Character Attributes” metric. From the error cases, we observe two failure patterns: (1) descriptions of the person often involve interactions with other objects (e.g., “holding a cat”); and (2) the clothing descriptions for the person are complex.

Regarding “Entity Relationships”, the error cases are often correlated with the “Character Attributes” issues. When an object’s attributes contain excessive errors, the evaluator will not recognize the object’s existence, leading to negative judgments. Additionally, errors occur when the object’s position deviates from conventional real-world placements.

Regarding “Scene Attributes”, this metric is relatively the simplest. Models typically generate accurate results as long as the supported prompt length is sufficient. For erroneous cases, aside from prompt truncation issues, failures primarily occur when: (1) the background contains excessive structural details, or (2) the style descriptions are specialized or uncommon.

N NEGATIVE CORRELATION BETWEEN PROMPT LENGTH AND ATTRIBUTE ALIGNMENT

In this section, we analyze the relationship between prompt length and attribute accuracy for the detected generated characters (categorized into objects, animals, and persons) to examine how the model’s attribute adherence vary with increasing prompt length. As illustrated in Figure 6, the left, middle, and right subgraph respectively show the attribute accuracy trends for “object”, “animal”, and “person” characters.

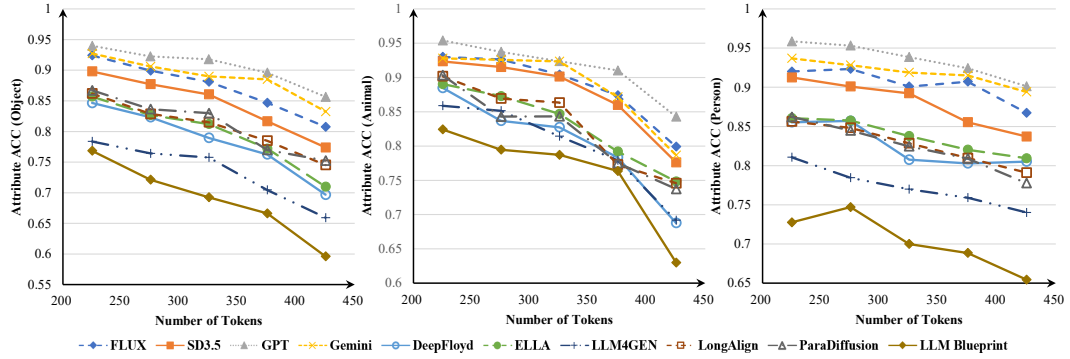


Figure 6: Negative correlation between prompt length and attribute alignment.

The trends show a clear inverse correlation between prompt length and attribute accuracy, indicating that longer prompts lead to progressively greater deviations from the intended character descriptions, manifested as attribute misalignment and omission. Notably, the performance comparison reveals that models specifically trained with long prompts (e.g., ELLA and ParaDiffusion) exhibit more gradual accuracy degradation compared to models using conventional training like Deepfloyd, as evidenced by their shallower accuracy decline curves. These findings collectively suggest that current text-to-image generation still face substantial challenges in maintaining attribute consistency under detail-intensive conditions, highlighting the critical need for further research into long-prompt optimization techniques and training methodologies to advance this crucial capability.

O LIMITATIONS

Regarding the quality of our benchmark data, we have conducted systematic sampling assessments involving professional annotators, validating the high quality of our dataset (detailed results presented in Appendix G). Section 5.1 further shows the substantial scale and diversity of our data, and Table 1 also provides comparative analyses highlighting its superior suitability for long-prompt scenarios relative to existing benchmarks. However, our current metrics, while extending T2I-CompBench’s metrics with “Character Locations” and “Scene Attributes”, remain potentially expandable through other dimensions such as aesthetic assessment or human preference scoring.

Regarding our evaluation protocol, it leverages LLMs as its core evaluation mechanism, which presents notable computational demands. The current implementation requires substantial GPU resources (minimum 20GB VRAM) and exhibits longer processing times compared to conventional evaluation methods. These resource-intensive characteristics may limit accessibility for some research teams. To address these constraints, we will investigate alternative evaluation methods that can maintain assessment accuracy while improving computational efficiency.

P CASE STUDIES

'polished_prompt': "A high angle shot of a brown wooden bench with several dishes on top of it. In the center and on the left are two round, wavy side plates with black scratches on the sides and a doily pattern engraved on the plates. On both plates is a thick brown cookie that's been crosscut at the top, located in the middle part of the image. The plate on the right has a candy with a yellow wrapper and green ends. To the right of the plates is a white mug with whipped cream on top that is similar to the glass plates. The cup, made of ceramic material, has a cylindrical shape with a handle and a textured surface. The white whipped cream on top is frothy and has an embossed design. Surrounding the wooden bench is a dark brown wooden floor. On the top right is a gray curtain, and on the upper left is a view of the lower part of a white wooden wall. The image is taken indoors with soft, warm lighting, likely from an overhead source, creating a cozy and inviting atmosphere. The lighting is evenly distributed, with no harsh shadows, suggesting a relaxed time of day, possibly evening. The style of the image is a realistic photo with a warm, homely aesthetic. The brown wooden bench supports the two round, wavy side plates with black scratches and a doily pattern, which are placed side by side. The thick brown cookies crosscut at the top are positioned on top of the two round, wavy side plates, with one cookie on each plate. The candy with a yellow wrapper and green ends is located on the right plate, next to the thick brown cookie. The white mug with whipped cream on top is situated to the right of the two round, wavy side plates. The two round, wavy side plates are adjacent to each other, with the plate containing the candy being closer to the white mug with whipped cream on top."

'character_attributes': [{"**main_character**": "brown wooden bench", "characteristics_list": ["several dishes on top"], "cls": "object"}, {"**main_character**": "two round, wavy side plates with black scratches and a doily pattern", "characteristics_list": ["two round, wavy side plates", "black scratches on the sides", "doily pattern engraved on the plates"], "cls": "object"}, {"**main_character**": "thick brown cookies crosscut at the top", "characteristics_list": ["thick brown cookie that's been crosscut at the top", "thick brown cookie"], "cls": "object"}, {"**main_character**": "white mug with whipped cream on top", "characteristics_list": ["white mug", "whipped cream", "ceramic material", "cylindrical shape", "handle", "textured surface", "frothy topping", "embossed design"], "cls": "object"}]

'character_locations': [{"**main_character**": "thick brown cookies crosscut at the top", "bbox": [765, 740, 820, 800], "position": "The middle part of the image"}]

'scene_attributes': [{"**scene_attribute**": "background", "content": "The background features a dark brown wooden floor and a white wooden wall with a gray curtain on the right side."}, {"**scene_attribute**": "light", "content": "The image is taken indoors with soft, warm lighting, likely from an overhead source, creating a cozy and inviting atmosphere. The lighting is evenly distributed, with no harsh shadows, suggesting a relaxed time of day, possibly evening."}, {"**scene_attribute**": "style", "content": "The style of the image is a realistic photo with a warm, homely aesthetic."}, {"**scene_attribute**": "spatial", "content": ["The brown wooden bench supports the two round, wavy side plates with black scratches and a doily pattern, which are placed side by side.", "The thick brown cookies crosscut at the top are positioned on top of the two round, wavy side plates, with one cookie on each plate.", "The candy with a yellow wrapper and green ends is located on the right plate, next to the thick brown cookie.", "The white mug with whipped cream on top is situated to the right of the two round, wavy side plates.", "The two round, wavy side plates are adjacent to each other, with the plate containing the candy being closer to the white mug with whipped cream on top."]}]

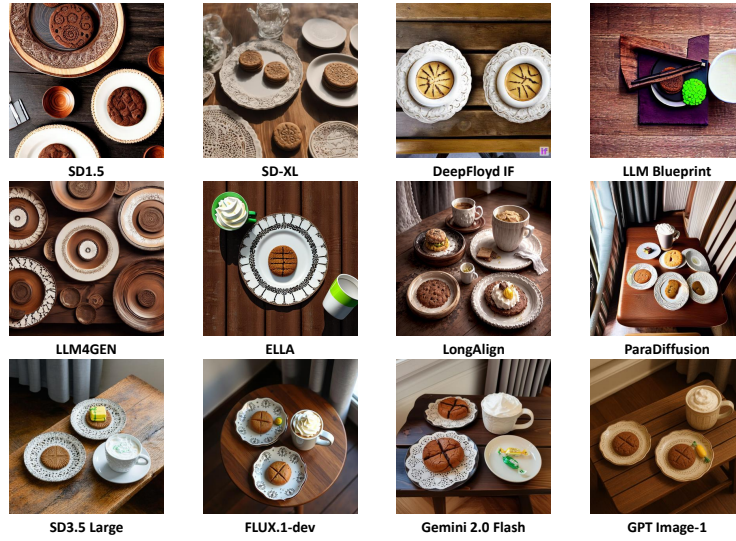


Figure 7: Comparative visualization set for case study 1.

The first challenging case study reveals that long-prompt optimized models exhibit superior completeness in main character generation compared to their backbone counterparts, with the four most advanced models achieving the highest fidelity. Regarding fine-grained details such as “crosscut at the top”, “cookies in the middle”, and “a gray curtain on the right side”, only the four most advanced models adhere to the instructions, with some remaining inaccuracies and omissions. While long-prompt optimized models (e.g., ParaDiffusion) interpret such details from the input, their generative capability remains constrained by backbone limitations, as evidenced by partial failures (e.g., generating cookies but omitting the crosscut).

'polished_prompt': 'A medium-close-up view of a small shed that is made up of light brown wooden planks that run vertically, and along these planks there are two rectangular openings that are round along the top. Inside the windows, there are brown wooden planks that run vertically. In between these openings there is a blue banner that has two drawings of an owl in the middle and a woman to the left who is facing the owl, and the owl is standing on the woman's arm. To the left of the window, there is another banner that is light blue, and along it there is black text that reads "WILDLIFE REVE" vertically. The roof of the shed is triangular and gray and is being lit up by the sun, with the light source positioned to the front-left, casting soft shadows on the shed. In the upper part of the image, in front of the roof, there is a small falcon that is flying across and to the left, with its sharp beak, outstretched wings, streamlined body, and feathered tail, showcasing its natural predator instincts and agile flight. The falcon is positioned above the light blue banner with black text '\WILDLIFE REVE'. Behind the shed is a tall tree that has a little bit of green foliage along it, and to the right of the tree are multiple trees that have no leaves along them. Behind the trees, a clear blue sky is visible, indicating a daytime setting in a natural or semi-natural environment. The image is brightly lit with natural sunlight, suggesting the light intensity is high, typical of midday. The style of the image is a realistic photo. It is daytime.'

'character_attributes': [{'main_character': 'small shed with light brown wooden planks and two arched openings', 'characteristics_list': ['made up of light brown wooden planks', 'planks that run vertically', 'two rectangular openings that are round along the top', 'brown wooden planks that run vertically inside the windows', 'triangular and gray roof', 'roof being lit up by the sun'], 'cls': 'object'}, {'main_character': 'blue banner with drawings of an owl and a woman', 'characteristics_list': ['blue banner', 'two drawings of an owl', 'woman to the left', 'facing the owl', 'owl is standing on the woman's arm'], 'cls': 'object'}, {'main_character': 'light blue banner with black text 'WILDLIFE REVE'', 'characteristics_list': ['light blue banner', 'black text', 'WILDLIFE REVE'], 'cls': 'object'}, {'main_character': 'small falcon flying in front of the shed', 'characteristics_list': ['animal', 'small falcon', 'flying', 'sharp beak', 'outstretched wings', 'streamlined body', 'in motion', 'feathered tail', 'agile flight'], 'cls': 'animal'}]

'character_locations': [{'main_character': 'small falcon flying in front of the shed', 'bbox': [674, 515, 906, 730], 'position': 'The upper part of the image'}]

'scene_attributes': [{'scene_attribute': 'background', 'content': 'The background features a clear blue sky and a mix of trees, some with green foliage and others bare, indicating a daytime setting in a natural or semi-natural environment.'}, {'scene_attribute': 'light', 'content': 'The image is brightly lit with natural sunlight, indicating a daytime setting, and the light source is positioned to the front-left, casting soft shadows on the shed. The clear blue sky suggests the light intensity is high, typical of midday.'}, {'scene_attribute': 'style', 'content': 'The style of the image is a realistic photo.'}, {'scene_attribute': 'spatial', 'content': ["The small falcon flying in front of the shed is positioned above the light blue banner with black text 'WILDLIFE REVE'.", "The blue banner with drawings of an owl and a woman is located between the two arched openings of the small shed with light brown wooden planks.", "The light blue banner with black text 'WILDLIFE REVE' is to the left of the blue banner with drawings of an owl and a woman.", "The small shed with light brown wooden planks and two arched openings is situated behind the small falcon that is flying in front of it."]}]



Figure 8: Comparative visualization set for case study 2.

The second challenging case study reveals systematic limitations across model categories: 1) Outdated models without long-prompt optimization fail to generate numerous specified characters, demonstrating catastrophic prompt adherence failures. 2) Long-prompt optimized models show improved yet incomplete character generation, indicating persistent architectural constraints. 3) Advanced models show critical shortcomings in detail fidelity. SD3.5 and FLUX fail to render the specified "blue banner with drawings of an owl and a woman", while Gemini 2.0 Flash and GPT Image-1 produce inaccurate textual elements ("WILDLIFE REVE"). These findings collectively underscore the ongoing challenges in compositional reasoning and detail preservation across current T2I models in long prompt scenarios.